Upconversion nanoparticles in biological labeling, imaging, and therapy

Feng Wang,[ab] Debapriya Banerjee,[a] Yongsheng Liu,[c] Xueyuan Chen[c] and Xiaogang Liu*[ab]

Upconversion refers to non-linear optical processes that convert two or more low-energy pump photons to a higher-energy output photon. After being recognized in the mid-1960s, upconversion has attracted significant research interest for its applications in optical devices such as infrared quantum counter detectors and compact solid-state lasers. Over the past decade, upconversion has become more prominent in biological sciences as the preparation of high-quality lanthanide-doped nanoparticles has become increasingly routine. Owing to their small physical dimensions and biocompatibility, upconversion nanoparticles can be easily coupled to proteins or other biological macromolecular systems and used in a variety of assay formats ranging from bio-detection to cancer therapy. In addition, intense visible emission from these nanoparticles under near-infrared excitation, which is less harmful to biological samples and has greater sample penetration depths than conventional ultraviolet excitation, enhances their prospects as luminescent stains in bio-imaging. In this article, we review recent developments in optical biolabeling and bio-imaging involving upconversion nanoparticles, simultaneously bringing to the forefront the desirable characteristics, strengths and weaknesses of these luminescent nanomaterials.

1. Introduction

The use of organic fluorophores as contrast agents for bio-imaging enables non-invasive detection and real-time visualization of biological processes at spatial scales from molecules to whole organisms.[1] Although optical bio-imaging with fluorophores has become the state of the art with the potential to impact fundamental biomedical research and clinical practice, it is not without limitation and complication. These fluorescent materials have broad emission spectra unsuitable for multiplex biolabeling and often suffer from photodegradation on exposure to external illumination. Quantum dots that feature a large molar extinction coefficient, high quantum yield, narrow emission bandwidth, size-dependent tunable emission and high photostability are attractive as alternative luminescent labels for optical labeling and imaging.[2–7] However, the use of quantum dots for biological detection is limited by several factors.[8] The potential toxicity of quantum dots that may pose risks to human

[a]Department of Chemistry, Faculty of Science, National University of Singapore, 3 Science Drive 3, Singapore 117543. E-mail: chmlx@nus.edu.sg
[b]Advanced Materials for Micro- and Nano-Systems Program, Singapore–MIT Alliance, Singapore 117576
[c]Key Laboratory of Optoelectronic Materials Chemistry and Physics, Fujian Institute of Research on the Structure of Matter, Chinese Academy of Sciences, Fuzhou, Fujian 350002, China
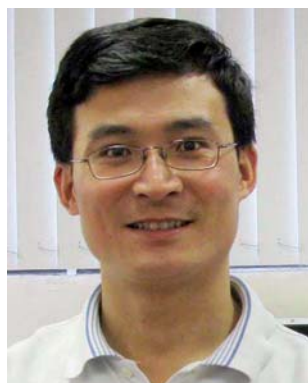
Feng Wang was born in Shaanxi, China. He received his BE (2001) and PhD (2006) degrees in Materials Science and Engineering from Zhejiang University. His PhD thesis was focused on the synthesis and characterization of lanthanide-doped fluoride nanomaterials under the supervision of Prof. Mingquan Wang and Prof. Xianping Fan. He joined the group of Prof. Xiaogang Liu at the National University of Singapore in 2007. His current research focuses on the synthesis, spectroscopic investigation, and application of luminescent nanomaterials.

Feng Wang

Debapriya Banerjee was born in Kolkata, India. She received her BS (2001) and MS (2003) degrees in Chemistry from Calcutta University. She completed her PhD (2009) in the field of ultrafast time-resolved spectroscopic techniques for biological macromolecules under the guidance of Prof. Samir Kumar Pal at the S. N. Bose National Centre for Basic Sciences. Subsequently, she joined the group of Prof. Xiaogang Liu at the National University of Singapore. Her present research interest lies in the field of luminescent nanomaterials.

Debapriya Banerjee

health and the environment under certain conditions has been a matter of much debate.[9] Intermittent emission (blinking)[10] also limits their use for labeling individual biological molecules. In addition, both the organic fluorophores and quantum dots are generally excited with ultraviolet (UV) and visible light. Absorption of UV and visible light by the biological samples often induces autofluorescence, which interferes with fluorescent signals obtained from exogenous biomarkers. Prolonged exposure of the biological samples to UV radiation can also cause sample photodamage and mutation.

The drawbacks of the Stokes-shifting dyes and quantum dots in biological applications have prompted the development of a new class of lanthanide-doped nanomaterials termed as upconversion (UC) nanoparticles. UC nanoparticles exhibit anti-Stokes emission upon low levels of irradiation in the near-infrared (NIR) spectral region, where biological molecules are optically transparent. In addition, these nanoparticles show a sharp emission bandwidth, long lifetime, tunable emission, high photostability, and low cytotoxicity,[11,12] which render them particularly useful for bio-imaging applications.

It should be noted that like organic dyes and quantum dots, lanthanide-doped nanoparticles can also display linear Stokes-shifted emission.[13–18] Although such nanoparticles have been utilized as luminescent probes in biological studies,[19–25] the need of UV excitation on these nanoparticles presents a significant limitation. As a separate note, most lanthanide emissions should refer to phosphorescence rather than fluorescence due to the involvement of spin-forbidden electronic transitions.[26] To avoid the misconception, the general term 'luminescence' will be used to describe UC emission.

In this review, we focus on the recent emergence of applications of lanthanide-doped UC nanoparticles in biological labeling, imaging, and therapy (Fig. 1). We discuss new technical advances that enable the current work along with the remaining limitations. The review is divided into four main sections. In the first section, we describe the basic principles of using UC nanoparticles as luminescent contrast agents. The applications of these nanomaterials for homogeneous and heterogeneous assays are discussed in the second section. The third section discusses the use of these nanomaterials as optical contrast agents for *in*

Fig. 1 Summary of biological applications of lanthanide-doped UC nanoparticles.

Yongsheng Liu received his BS degree (2001) in Chemistry from Shandong Normal University and his MS degree (2007) in Physical Chemistry from Fujian Institute of Research on the Structure of Matter (FJIRSM), Chinese Academy of Sciences. He is currently pursuing his PhD at FJIRSM mentored by Prof. Xueyuan Chen. His research interest focuses on the synthesis and optical spectroscopy of lanthanide-doped luminescent nanomaterials.

Yongsheng Liu

Xueyuan Chen earned his BS degree (1993) from University of Science and Technology of China and his PhD (1998) from Fujian Institute of Research on the Structure of Matter (FJIRSM), Chinese Academy of Sciences. From 2001 to 2005 he was a postdoctoral research associate at the Chemistry Division of Argonne National Laboratory, U.S. Department of Energy, where he studied the photophysics and photochemistry of heavy elements. In 2005, he joined the faculty at FJIRSM, where he is currently professor and group leader in Material Chemistry and Physics. His research focuses on optical spectroscopy and bio-applications of lanthanide-doped luminescent nanomaterials.
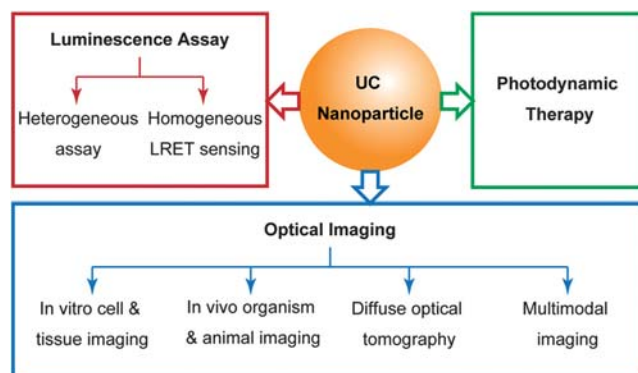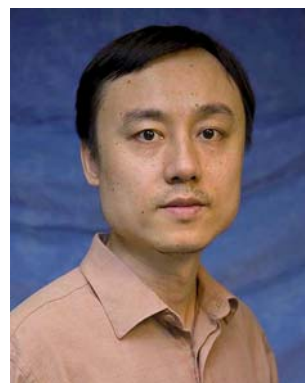
Xueyuan Chen

Xiaogang Liu was born in Jiangxi, China. He earned his BE degree (1996) in Chemical Engineering from Beijing Technology and Business University. He received his MS degree (1999) in Chemistry from East Carolina University under the direction of Prof. John Sibert and completed his PhD (2004) at Northwestern University under the supervision of Prof. Chad Mirkin. He then became a postdoctoral fellow in the group of Prof. Francesco Stellacci at MIT. He joined the faculty of the National University of Singapore in 2006. His research interests include nanomaterials synthesis, supramolecular chemistry, and surface science for catalysis, sensors and biomedical applications.

Xiaogang Liu

This journal is © The Royal Society of Chemistry 2010

vitro and *in vivo* imaging and diffuse optical tomography. The recent advances of these nanoparticles for multimodal imaging are also encompassed and described in this section. In the last section, we review the progress made and the future prospects for the use of these nanoparticles in photodynamic therapy.
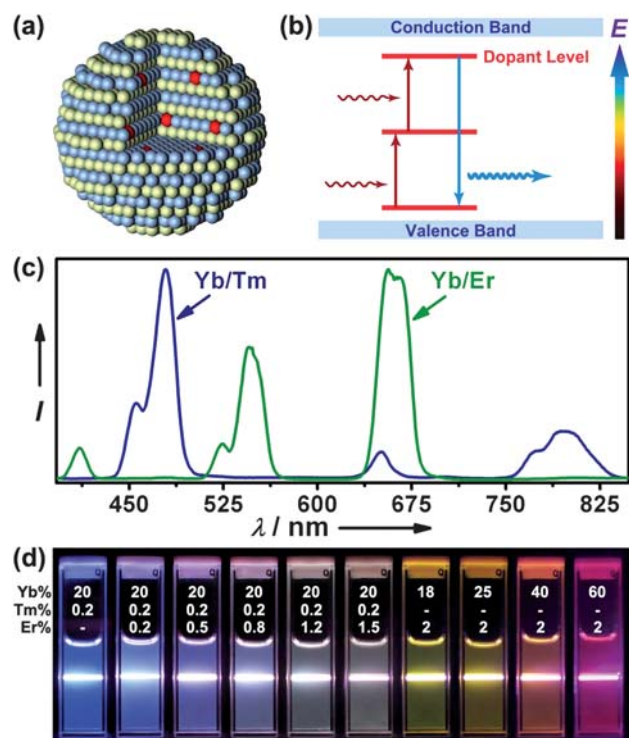

Fig. 2 Structure and optical properties of UC nanoparticles. (a) Schematic illustration of UC nanoparticles composed of a crystalline host and lanthanide dopant ions embedded in the host lattice. (b) Schematic energy level diagram showing that UC luminescence primarily originates from electron transitions between energy levels of localized dopant ions. (c) Typical emission spectra showing multiple narrow and well-separated emissions produced by cubic $NaYF_4$:Yb/Tm (20/0.2 mol%) and $NaYF_4$:Yb/Er (18/2 mol%) nanoparticles. (d) UC multicolor fine-tuning through the use of lanthanide-doped $NaYF_4$ nanoparticles with varied dopant ratios. Note that the emission spectra and colors are associated with the host composition, particle size, and particle surface properties. (Emission spectra and luminescent photos are reprinted with permission from ref. 105. Copyright 2008, American Chemical Society.)

2. Properties of upconversion nanoparticles

In stark contrast to the conventional luminescence processes that typically involve one ground state and one excited (emitting) state, UC processes rely on the existence of multiple intermediate states to accumulate the low-energy excitation photons. A variety of optical processes, including excited-state excitation, energy transfer upconversion, and photon avalanche, are responsible for UC emission.[27] All these processes occur through sequential absorption of two or more photons within energy states of a dopant ion in the crystalline particle. Luminescent materials featuring f- and d-ions that have more than one metastable level can principally be used to generate UC luminescence.[28] However, efficient UC processes only occur with trivalent lanthanide ions owing to their extremely long-lived intermediate energy states.[29,30]

2.1 Composition and crystallinity

UC nanoparticles generally comprise an inorganic host and lanthanide dopant ions embedded in the host lattice (Fig. 2a). Although UC emission can be theoretically expected from most lanthanide ions, visible optical emissions under low pump power densities (*ca.* 10 W/cm²) are only generated by using Er^{3+}, Tm^{3+}, and Ho^{3+} as activators. The selection of these dopants is due to their equally spaced energy levels that facilitate photon absorption and energy transfer steps involved in UC processes. To enhance UC efficiency, Yb^{3+} with a larger absorption cross-section in the NIR spectral region is frequently doped as a sensitizer in combination with the activators. As a rule of thumb, in a sensitizer–activator system the doping level of the activator is kept below 2 mol% to minimize the loss of excitation energy by cross-relaxation process.[31]

UC processes primarily rely on the ladder-like arrangement of energy levels of lanthanide dopant ions (Fig. 2b). However, in the realization of efficient UC processes, the crystal structure and optical property of host materials play important roles and require careful consideration. Excited energies of the dopant ions may be absorbed by the host materials through lattice vibrations.[32,33] Variation of the crystal structure in the host materials also alters the crystal field around the dopant ions, resulting in different optical properties of the nanoparticles.[34–36] Desirable host materials should have adequate transparency within the wavelength range of interest, low phonon energy and high optical

Table 1 Typical UC host materials and their synthetic strategies

UC host[a]	Synthetic strategy						
	Co-precipitation[b]	Hydro(solvo)thermal processing	Thermal decomposition	Two-phase synthesis	Combustion synthesis	Ionic liquid-based synthesis	Microwave-assisted synthesis
Y_2O_3	Ref. 61		Refs. 62–64		Refs. 65, 66		
Y_2O_2S	Ref. 67				Ref. 68		
LaF_3	Refs. 69, 70	Refs. 71, 72	Ref. 73	Ref. 74			
$NaYF_4$	Refs. 35, 75, 76	Refs. 77–81	Refs. 82–85	Refs. 86, 87		Refs. 88–90	Refs. 91–93
$NaGdF_4$	Ref. 94	Ref. 95	Refs. 96, 97	Ref. 98			

[a] Only host materials that are commonly used in biological studies are listed here. For comprehensive lists of the host materials, please refer to refs. 30 and 99–101. [b] Co-precipitation synthesis typically requires a post-heat treatment to increase the crystallinity of the nanoparticles for enhanced UC emission.

damage threshold. In addition, the host materials should have close lattice matches to dopant ions for achieving high doping levels. In these regards, inorganic compounds of rare earth ions, alkaline earth ions, and a number of transition metal ions (e.g. Zr^{4+}, Ti^{4+}, and Mn^{2+}) are suitable host materials for lanthanide dopant ions.[37–60] Table 1 is a list of host materials commonly used in UC-based biological studies.

Although most UC nanoparticles can be synthesized by a variety of methods, considerable effort has been devoted to developing methods that yield highly crystalline structures for highly efficient UC emission. Nanoparticles with well-crystallized structures exert a strong crystal field around the dopant ions and minimize the energy loss of the dopant ions arising from crystal defects. For biological application, nanoparticles should also have a small particle size and high dispersity for integration with biological molecules and macromolecules. Conventional techniques for synthesizing UC nanoparticles with high crystallinity, dispersity, and well-defined crystal phase and size generally require control over a set of conditions, such as high reaction temperature and prolonged reaction time.[102] However, these treatments can lead to particle aggregation or enlarged particle size. We have recently developed conditions which allow the facile formation of $NaYF_4$ UC nanocrystals with small feature size and desirable optical properties.[102] By careful doping with Gd^{3+} ions at different concentrations, we observed phase- and size-variation of the nanocrystals, which was also confirmed in another recent paper by Yu et al.[103]

2.2 Optical properties

The absorption and emission spectra of lanthanide ions primarily arise from intra-configurational $4f^n$ electron transitions. Shielded by the completely filled $5s^2$ and $5p^6$ sub-shells, the 4f electrons hardly experience interactions with the host lattice. The absorption and emission spectra of lanthanide-doped nanoparticles therefore show sharp lines (10–20 nm full width at half maximum) and resemble the spectra of free ions. One drawback of the narrow absorption profile is that it imposes certain constraints on the selection of the excitation source. Fortunately, commercially available InGaAs diode laser systems operate at a wavelength of ca. 980 nm that well matches the absorption of Yb^{3+}, providing an ideal excitation source for UC nanoparticles.

Lanthanide ions typically show a distinct set of sharp emission peaks, thus providing distinguishable spectroscopic fingerprints for accurate interpretation of the emission spectra in the event of overlapping emission spectra (Fig. 2c). The emission peak wavelength of UC nanoparticles is essentially independent of the chemical composition or physical dimension of the host materials. Their emission colors are usually manipulated by control of either the emission wavelength or relative emission intensities through control of host/dopant combinations and dopant concentrations (Fig. 2d).[32,33,104–111]

Compared to conventional anti-Stokes processes such as second harmonic generation and multiphoton absorption, UC emission is based on the physically existing states, thus allowing more efficient frequency conversion.[28–30] In general, UC processes can be induced by a low power (1–10^3 W/cm²) continuous wave laser, as opposed to a costly high-intensity
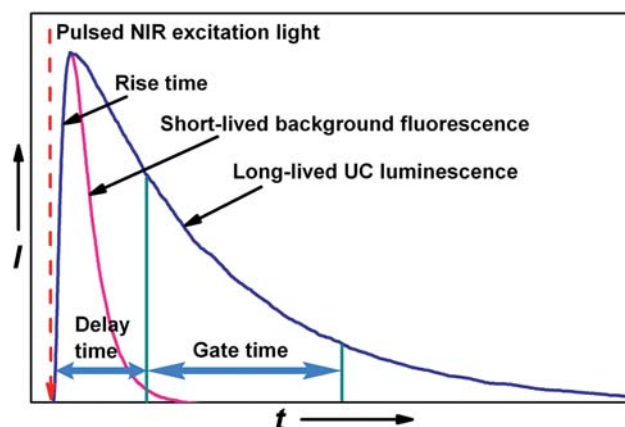

Fig. 3 The measurement principle of the time-resolved luminescence detection technique based on UC nanoparticles. The short-lived background fluorescence can be effectively eliminated by setting an appropriate delay time and gate time. The long-lived UC luminescence of trivalent lanthanide ions is collected during the gate time.

(10^6–10^9 W/cm²) pulsed laser source for the generation of a simultaneous two-photon process.

UC emission arising from intra-4f electron transitions of lanthanide ions does not involve the breaking of chemical bonds. The nanoparticles are therefore stable against photobleaching and photochemical degradation. Several independent studies have revealed that the luminescence properties of lanthanide-doped nanoparticles remain essentially unaltered after continuous irradiation by UV lamp or NIR laser for hours.[75,112–114]

UC nanoparticles also emit light constantly against optical blinking. Although blinking was observed for individual lanthanide ions,[115] UC nanoparticles that commonly contain a large number of lanthanide dopant ions do not blink under continuous irradiation of a NIR laser, which has been recently experimentally confirmed.[97,116]

Since the f–f electron transitions are Laporte-forbidden, the UC process of trivalent lanthanide ions is usually characterized by a long luminescence lifetime. This optical feature makes the time-resolved luminescence detection technique readily feasible to minimize the interference of the undesired short-lived background fluorescence that occasionally originates from biological tissues, organic species, or other dopants under multiple-photon excitation. When compared to the conventional steady-state luminescence detection technique, this technique offers a remarkably higher detection sensitivity due to significantly improved signal-to-noise ratios (Fig. 3).

2.3 Surface chemistry

UC nanoparticles are typically prepared in the presence of capping ligands that control particle growth and stabilize the particles against aggregation in solutions. Immobilized surface ligands containing functional groups can provide easy access to nanoparticles for subsequent biological functionalization.[22,50,78,95,105,117–119] However, most UC nanoparticles prepared by conventional strategies have either no intrinsic aqueous solubility or lack functional organic moieties. Therefore, an additional surface treatment step prior to bioconjugation is
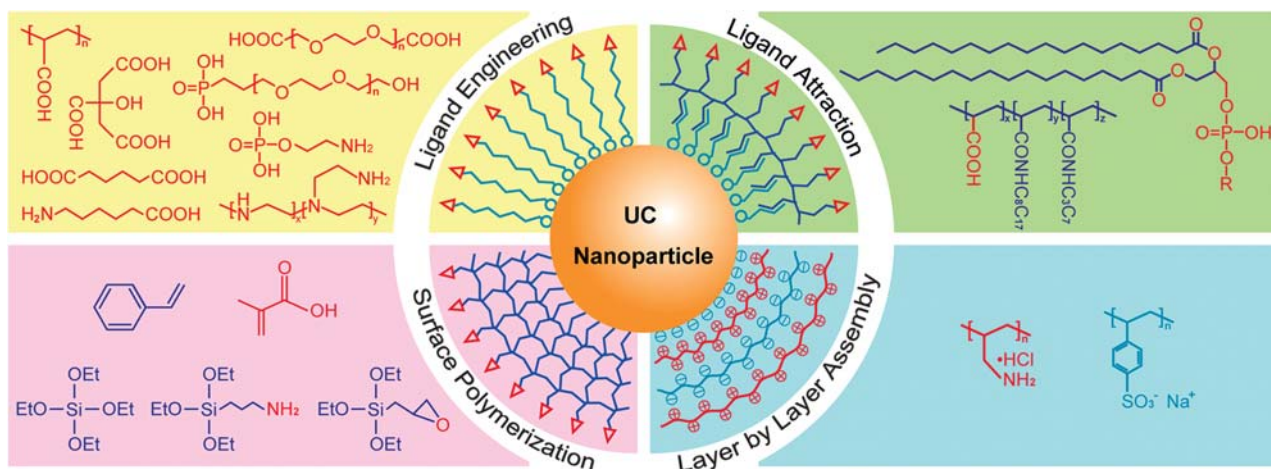
Fig. 4 Typical strategies and surface molecules (monomers) used for making hydrophilic UC nanoparticles with pendant functional groups. Ligand engineering involves a ligand exchange reaction with hydrophilic bifunctional molecules or involves a direct oxidation of the terminal group of native ligands to generate a pendant carboxylic functional group. Some bifunctional molecules may be employed in a one-pot synthetic procedure to directly yield hydrophilic UC nanoparticles with additional functional groups and further bioconjugation capabilities. Ligand attraction involves absorption of an additional amphiphilic polymer onto the nanoparticle surface through the hydrophobic van der Waals attraction between the original ligand and hydrocarbon chain of the polymer. Layer-by-layer assembly involves electrostatic absorption of alternately charged polyions on the nanoparticle surface. Surface polymerization involves growing a dense cross-linked shell on the nanoparticle core by condensation of small monomers.

required. Fig. 4 provides a summary of the representative strategies for surface modification of lanthanide-doped UC nanoparticles.

A common approach to generating a pendant functional group on the surface of nanoparticles is ligand engineering that involves a ligand exchange reaction or an oxidation of the native ligand. For example, hydrophobic ligands on the surface of the as-prepared nanoparticles can be replaced through ligand exchange reactions by a wide variety of hydrophilic organic molecules including 6-aminohexanoic acid (AHA),[20] poly-(ethylene glycol) (PEG) diacid,[84] hexanedioic acid (HDA),[120] citrate,[121] polyacrylic acid (PAA),[86,96,122,123] and phosphate-derived molecules.[124,125] Alternatively, native capping ligands containing monounsaturated carbon–carbon double bonds can be directly oxidized into carboxylic acid groups.[96,126–129]

Apart from ligand engineering, surface functionalization of UC nanoparticles has been achieved through ligand attraction, electrostatic layer-by-layer assembly, and surface polymerization (Fig. 4). Several types of materials including amphiphilic polymers,[116,130,131] linear polyions,[132] styrenes,[133] and silanes.[19,69,75,76,79,85,86,134–139] have been used to form water-soluble core–shell UC nanoparticles. Important for these methods is the surface coverage with molecules consisting of additional functional groups that allow further reactions with biological entities. Among various surface-coating methods, silica coating enjoys common usage by several groups, partly due to the well-established surface chemistry of silica coating for facile bioconjugation. Another reason perhaps lies in that the silica coating is readily applicable to both hydrophilic and hydrophobic nanoparticles *via* the Stöber method and reverse-microemulsion method, respectively. Reverse-microemulsion method was first demonstrated by Shan and Ju[85] to coat hydrophobic NaYF$_4$:Yb/Er nanoparticles. Recently, van Veggel and co-workers[139] have developed a two-step silica-coating procedure to solve the problems associated with excess surfactants involved

in the reverse-microemulsion method. They showed that hydrophobic NaYF$_4$:Yb/Er nanoparticles can be coated with silica by the Stöber method after ligand exchange with polyvinylpyrrolidone.

Although laborious to some extent, the coating methods usually lead to highly stable colloidal particles in comparison with the ligand engineering method. Another distinctive feature of these methods is the retention of the native surface structures, thereby reducing the possibility of creating surface defects that quench the UC luminescence. Caution should, however, be exercised in selecting coating molecules since surface modification sometimes adversely affects their photophysical properties. For lanthanide resonance energy transfer (LRET) assays, the shell thickness of the coated particles has to be minimized.

2.4 Cytotoxicity

With the rapid progress in developing biological applications of UC nanoparticles, there is a pressing demand for assessment of the potential hazards of these nanomaterials to humans and other biological systems. Cytotoxicity is a rapid, standardized test that is a very sensitive and low-cost way to determine if the UC nanoparticles contain quantities of harmful components.

Cytotoxicity tests through evaluations of cellular morphology and mitochondrial function (MTT and MTS assays) show that lanthanide-doped nanoparticles are non-cytotoxic to a broad range of cell lines.[78,97,118,119,123,129,140–143] To determine their cytotoxicity, the nanoparticles are first incubated with cells at various particle concentrations and incubation times. The cells' viability is then scored for cytotoxic effect under control and exposed conditions. For example, Li and co-workers[129,141] have examined the biocompatibility of Yb/Er-doped rare earth fluorides coated with a silica shell or a layer of azelaic acid molecules. They found that these nanoparticles had essentially no effect on the cell viability of human nasopharyngeal epidermal carcinoma KB
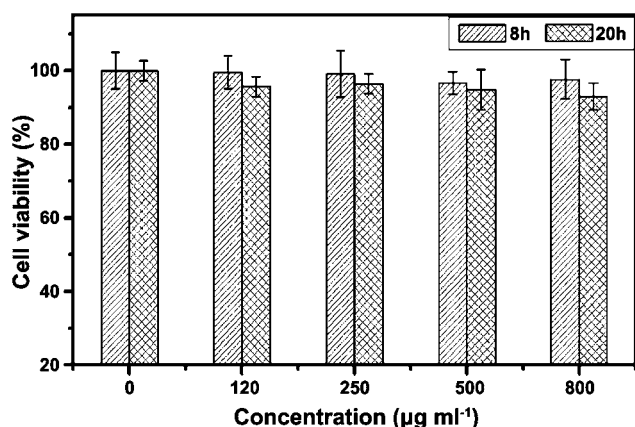
Fig. 5 *In vitro* cell viability of KB cells incubated with SiO₂-coated NaYF₄:Yb/Er nanoparticles at different concentrations for 8 or 20 h. (Reprinted with permission from ref. 141. Copyright 2009, Wiley-VCH Verlag GmbH & Co. KGaA.)

cells after incubation for 20 h at a particle concentration of 800 μg/ml (Fig. 5). Shan *et al.*[140] have also reported that there is limited or no toxicity of carboxyl- and amino-functionalized nanoparticles after incubation for 9 days with human osteosarcoma cells. In a separate report, Tan and co-workers[143] have showed that lanthanide-doped Y₂O₃ nanoparticles are biocompatible to hepatoma HepG2 and fibroblast NIH 3T3 cells.

The cytotoxicity of UC nanoparticles performed *in vivo* was also assessed by animal studies. Recent work by Jalil and Zhang[142] showed that healthy rats, injected intravenously with silica-coated NaYF₄:Yb/Er nanoparticles with a dosage of 10 mg/kg of body weight, exhibited no signs of weight loss or abnormal behavior after 7 days. The biodistribution of nanoparticles in different organs was also investigated after intravenous injection at different time intervals. The injected dose was mostly excreted by the rats through their urine or faeces after 7 days. However, to ensure the suitability of the UC nanoparticles for *in vivo* biological applications, further long-term (up to several months) toxicity studies concerning particle size, shape, and surface chemistry are necessary.

3. As luminescent reporters for sensitive assay

UC labeling through the use of lanthanide-doped nanoparticles seeks to minimize photodamage to the biomolecules and to substantially reduce background autofluorescence. Therefore, the use of UC nanoparticles as luminescent labels provides enhanced signal-to-noise ratios and thus improved limits of detection as compared to conventional fluorophores.

3.1 Heterogeneous assay

A heterogeneous assay platform utilizes molecules that are bio-functionalized and captured on a solid substrate. Target analytes, which are present in a sample comprising UC particle labels, are incubated on the substrate, washed, and detected by NIR diode laser irradiation. The concentration of the target analyte can be quantified by measuring the UC emission intensity (Fig. 6). As the heterogeneous assay platform does not need
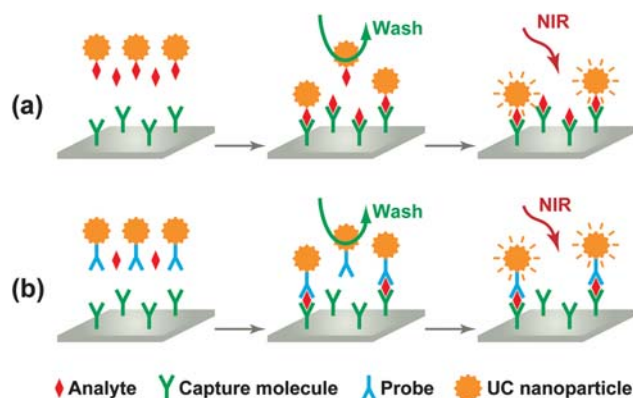

Fig. 6 Schematic illustrations of heterogeneous assays involving UC particles. (a) Competitive assay. (b) Non-competitive (sandwich) assay. In a competitive assay, the analyte competes with labeled probes to bind to the capture molecule. The optical response will be inversely proportional to the concentration of the analyte. In a non-competitive assay, the analyte is first bound to the capture molecule, while the labeled probe is bound to the analyte. Consequently, the results will be directly proportional to the concentration of the analyte.

precise control of the particle–biomolecule distance, this type of application is generally not limited by the size of the particles and is less susceptible to interference caused by surface coating of the particles.

UC particles have been previously demonstrated in immunoassays as alternatives to conventional labeling agents.[144–148] For example, submicron-sized Y₂O₂S particles doped with Yb³⁺ and Er³⁺ ions have shown a detection limit of 10 pg human chorionic gonadotropin in a lateral flow (LF) immunochromatographic assay format.[144] In contrast to conventional labeling agents such as gold nanoparticles or colored latex beads, the UC particles exhibit a 10-fold improvement in detection sensitivity. Another intriguing example has been demonstrated by Niedbala *et al.*,[145] who developed an LF-based strip assay for the simultaneous detection of amphetamine, methamphetamine, phencyclidine, and opiates in saliva by using multicolor UC particles (Fig. 7). In their study, green-emitting (550 nm) particles were coupled to antibodies for phencyclidine and amphetamine, while blue-emitting (475 nm) particles were coupled to antibodies for methamphetamine and morphine. By analyzing the test strip for
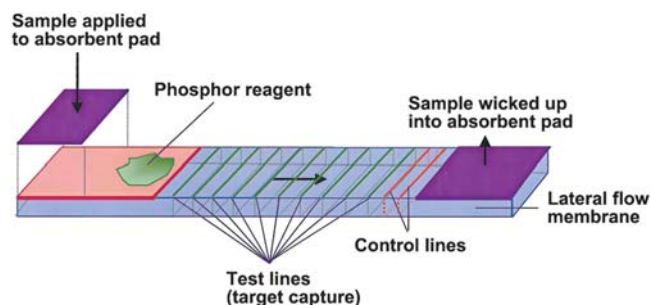

Fig. 7 UC-based lateral flow format developed by Niedbala *et al*. The architecture of the lateral flow strip is designed to accommodate up to 12 distinct test lines. In addition, each strip also contains two control lines. (Reprinted with permission from ref. 145. Copyright 2001, Elsevier B.V.)
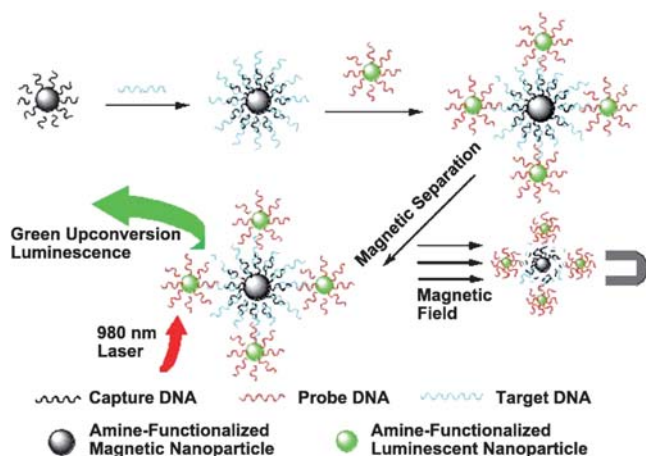
Fig. 8 Scheme of the UC nanoparticle-based DNA detection. Magnetic nanoparticles are used and modified with capture DNA strands. UC nanoparticles are modified with probe DNA strands. Upon incubation with target DNA strands, the UC and magnetic nanoparticles form binary nanoparticle aggregates. The aggregates can be purified with magnetic separation and examined *via* UC luminescence assays. (Reprinted with permission from ref. 153. Copyright 2006, Royal Society of Chemistry.)

each colored phosphor, the drug molecules were successfully detected on the basis of phosphor color and position.

UC particles have also been used as luminescent reporters in genomic applications. Due to the elimination of unwanted autofluorescence, UC particles can facilitate the detection and handling of target molecules by shortening the polymerase chain reaction (PCR) amplification process. For example, Corstjens *et al.*[149] have demonstrated in LF-based DNA detection that one target DNA can generate a positive signal after completion of only 20 PCR amplification cycles through use of UC particle reporters. In a parallel development, Zuiderwijk *et al.*[150] have shown that the use of UC particle reporters even allows identification of the bacterial pathogen *Streptococcus pneumoniae* without PCR or other amplification techniques. The potential of UC particle reporters has also been exploited by Tanke and co-workers[67] to achieve a detection limit of 1 ng/μl oligonucleotides by using 400-nm Y_2O_2S:Yb/Er particles.

Although submicron-sized UC particles work well for most heterogeneous assays, smaller particles with a decreased number of probe molecules per particle should result in better target-to-reporter ratios and improved assay kinetics.[151,152] Recently, Wang and Li[153] have demonstrated a sandwich-hybridization assay for the ultra-sensitive detection of DNA using sub-50-nm $NaYF_4$:Yb/Er nanoparticles (Fig. 8). When combined with magnetic nanoparticles for facile separation, this method has shown a detection limit of *ca.* 10 nM without PCR amplification.

3.2 Homogeneous assay

UC-based homogeneous assays are commonly based on a lanthanide resonance energy transfer (LRET) process between a donor and an acceptor (Fig. 9). Unlike heterogeneous assays, homogeneous assays make use of binding-modulated signals, eliminating the need of separating un-bound labels.
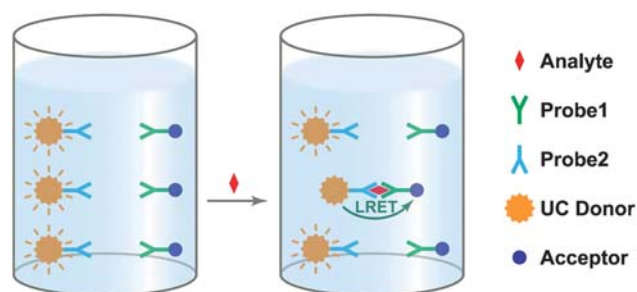

Fig. 9 Schematic of an LRET-based homogeneous sandwich assay system. The system involves the use of UC particles as energy donors and other optical materials as energy acceptors. When the donor and acceptor are linked in close proximity in the presence of the analyte, LRET results in a variation in optical signal. As the dipole–dipole interaction described by LRET is strongly dependent on donor–acceptor separation, un-bound labels do not need to be removed from the system.

Consequently, they are easier to automate and faster to perform. However, owing to the short-range optical process of LRET, small-sized particles with thin layers of surface coatings are required to provide a proximal contact between the donor and the acceptor for efficient energy transfer.[154]

As a derivative of fluorescence resonance energy transfer (FRET), LRET was first introduced as luminescence resonance energy transfer by Selvin *et al.*[155] when utilizing lanthanide-chelated complexes in FRET studies. LRET relies on the same dipole–dipole mechanism as conventional FRET, but offers a number of technical advantages including large energy transfer distance range (>10 nm) and high reliability. Particularly, the long-lived luminescent lanthanide donors allow facile and accurate lifetime measurements to monitor biological events that are inaccessible with conventional fluorescent dyes.[156] LRET is now widely used to describe a FRET system involving a lanthanide-based luminescent donor.

The application of UC particles to LRET-based bioassays was first proposed by Morgan and Mitchell.[157] The concept was later
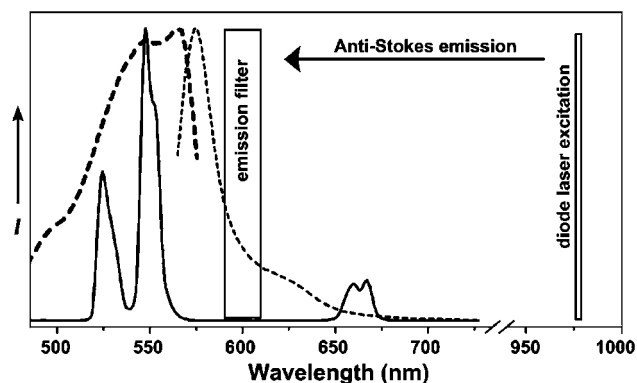

Fig. 10 Emission spectrum of the Yb/Er-doped UC phosphor and emission and excitation spectra of BPE. The emission spectrum of the UC phosphor (solid line) overlaps with the excitation spectrum of BPE (dark dashed line). The emission spectrum of BPE (light dashed line) is separated from the phosphor emission, and the sensitized emission of BPE can be measured at 600 nm using a band-pass emission filter and continuous laser excitation at 980 nm. (Reprinted with permission from ref. 158. Copyright 2005, American Chemical Society.)

experimentally proved by Kuningas et al.,[158] who demonstrated the detection of biotin by utilizing streptavidin-conjugated UC phosphors as the donors and biotinylated phycobiliprotein (bio-BPE) as the acceptor. Importantly, the use of UC phosphors as the LRET energy donors displays a remarkable advantage over traditional quantum dots and organic dyes in that NIR irradiation is absorbed by the UC particles, but not by the acceptor. False detection signals resulting from direct absorption by the acceptor under UV excitation can be avoided. Furthermore, owing to the extremely narrow and sharp emission bands of lanthanide dopant ions, practically no donor emission is detectable at the wavelength range where acceptor emission is investigated (Fig. 10).

Simultaneous detection of multiple analytes by using multi-peak emission profiles of UC particle donors has also been demonstrated by Rantanen et al.[159] In a dual-parameter sandwich-hybridization assay (Fig. 11), two probe oligonucleotides (P1 and P2) with sequences complementary to a target sequence of β-actin (T1) or HLA-B27 (T2) were selectively conjugated to Alexa Fluor 546 (AF546) and Alexa Fluor 700 (AF700). The oligonucleotide-modified dye molecules and target oligonucleotides were then mixed with UC particles pre-modified with capture oligonucleotides (C1 or C2). Upon formation of the sandwich complex through hybridization, the donor emissions at 540 and 653 nm were quenched by AF546 and AF700, respectively. By measuring the intensities of probe-specific emissions at 600 and 740 nm, two different target–oligonucleotide sequences can be detected simultaneously and quantified with a dynamic range of measurement from 0.35 to 5.4 nM.

One major drawback of the aforementioned works is the use of rather large-sized UC particles as the energy donors. Because only emissive dopant ions located near the particle surfaces can participate in the LRET, a considerably large fraction of emissive ions embedded in the core structures produces signals only through non-proximity-based reabsorptive energy transfer.[158,160–162] In addition, large particles of low analyte density result in a limited dynamic range of measurement.[159] By utilizing small-sized UC nanoparticles, a hybridization-based DNA assay with an unoptimized dynamic range of 0–60 nM has recently been demonstrated by Zhang et al.,[163] who further showed that
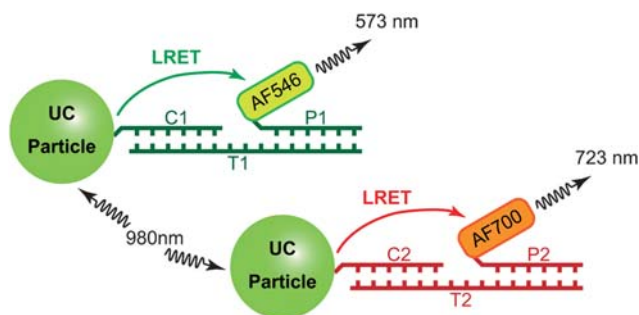
Fig. 11 Principle of the dual-parameter sandwich-hybridization assay system reported by Rantanen et al. Two types of dye probes were used to quench the UC particle emission at 540 nm and 653 nm, respectively. After the formation of the sandwich complex, the probe-specific emission signals are directly related to the presence of corresponding targets. (Reprinted with permission from ref. 159. Copyright 2009, Royal Society of Chemistry.)
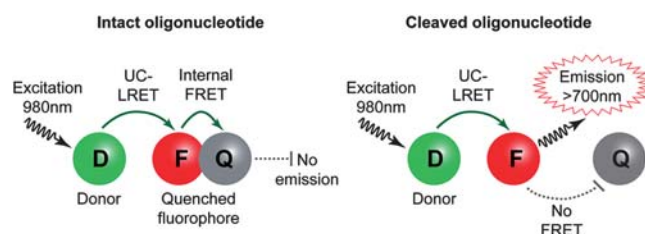
Fig. 12 Principle of the homogeneous enzyme-activity assay system. The hydrolytic enzyme reaction separates the fluorophore (F) and the quencher (Q) located at different ends of the oligonucleotide and so the emission of the fluorophore (measured at >700 nm) is recovered. Intact oligonucleotides remain non-fluorescent. (Reprinted with permission from ref. 167. Copyright 2008, Wiley-VCH Verlag GmbH & Co. KGaA.)

oligonucleotide-modified UC nanoparticles can distinguish target DNAs with single-base mismatches.[164,165] Chen et al.[126] also reported DNA detection range of 10–50 nM by making use of sub-15-nm UC nanoparticles.

Recently, Wang et al.[132] have developed a highly sensitive biosensor for the detection of avidin using sub-50-nm NaYF$_4$:Yb/Er nanoparticles. Instead of using organic dyes, they utilized metallic nanoparticles as the energy acceptors or quenchers for donor–acceptor energy transfer. By using 7 nm gold nanoparticles, this method registers an unoptimized detection limit of 0.5 nM. In a parallel development, Xu and co-workers[166] have reported a sandwich LRET system comprising human immunoglobulin G (IgG)-modified NaYF$_4$:Yb/Er nanoparticles as the energy donors and rabbit anti-goat IgG-modified gold nanoparticles as the energy acceptors. The system offers a substantially low detection limit of 0.88 μg/ml for goat anti-human IgG, providing potential use for the trace detection of a variety of biomolecular analytes.

An intriguing recent development was demonstrated by Rantanen et al.,[167] who combined UC-based LRET with conventional FRET for a fluorescence-quenching-based enzyme-activity assay (Fig. 12). The system design involves the use of an Alexa Fluor 680 (AF680) fluorophore to receive upconverted energy and the use of a Black-Berry Quencher 650 (BBQ650) to quench AF680-emitted fluorescence. The AF680 and BBQ650 fluorophores are linked to the 5′- and 3′-ends of a single-stranded oligonucleotide sequence, respectively. Upon an enzymatic reaction catalyzed by benzonase endonuclease, the oligonucleotide is cut into shorter fragments, resulting in recovered emission of AF680. In comparison with a conventional method that relies on direct excitation into AF680 at 655 nm, the UC-based method offers an 8-fold increase in signal-to-background ratio.

4. As contrast stains for optical imaging

As UC is more efficient than multiphoton processes, a common optical microscope can be readily used for UC imaging with a xenon lamp adapted to a diode laser. Thus, the UC particle-based imaging approach is technically superior to conventional NIR multiphoton microscopy that requires a complex experimental setup and expensive pulsed lasers.[168–170] This attribute makes UC particles particularly convenient as contrast stains for optical imaging.

4.1 In vitro cell and tissue imaging

Zijlmans et al.[171] first exploited upconverting properties of lanthanide-doped particles for high performance bio-imaging. In their influential paper published in 1999, submicron-sized Y_2O_2S:Yb/Tm particles were used to study the distribution of prostate-specific antigen (PSA) in paraffin-embedded sections of human prostate tissue using standard immunohistological techniques. They showed that the non-specific autofluorescence signal associated with short-wavelength excitation was completely eliminated under NIR excitation (Fig. 13a). Moreover, it was demonstrated that UC particle reporters do not bleach after continuous exposure to high excitation energy levels. Therefore, UC particle labeled tissue samples can be conveniently stored for permanent records.

In recent years, when high-quality UC nanoparticles became readily available, the UC-based imaging technique has been widely used for high-resolution imaging of cellular specimens. Non-functionalized UC nanoparticles incubated with a variety of cell lines are found to be endocytosed by the cells.[97,113,116,121,125,127,140,142,172,173] Upon 980-nm excitation, strong UC luminescence is clearly observed in cells without autofluorescence (Fig. 13b).[116] Owing to their inherent high photon conversion efficiency and non-blinking emission behavior, UC nanoparticles even allow reliable single-molecule imaging that challenges conventional staining agents.[97,116,140] Importantly, Yu et al.[113] have demonstrated that the UC-based visualization technique has negligible fading effect over time (Fig. 13c),
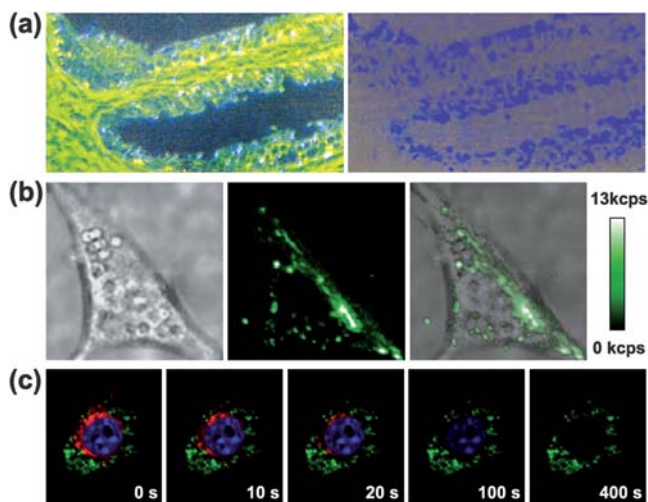

Fig. 13 Imaging tissue and cells with UC nanoparticles. (a) Tissue section after exposure to both blue and NIR excitation light (left); the green autofluorescence that coincides with the PSA-specific blue phosphor luminescence can be effectively eliminated using only NIR excitation (right). (b) Live-cell image of NIH 3T3 murine fibroblasts with endocytosed $NaYF_4$:Yb/Er nanoparticles: the left, middle, and right columns are brightfield, luminescence, and overlay images, respectively. (c) Comparison of photobleaching of UC nanoparticles and organic dyes in confocal microscopy imaging: excitation was provided by continuous-wave lasers at 405, 543, 980 nm with powers in the focal plane of approximately 1.6, 0.13 and 19 mW, respectively. (Reprinted with permission from: (a) ref. 171, (b) ref. 116, and (c) ref. 113. Copyright 1999, 2009, 2009, respectively, Elsevier B.V., National Academy of Sciences, USA, and the American Chemical Society.)

implying extraordinary ability of UC nanoparticles for long-period observation of cells.

Target imaging of tumor cells has also been widely investigated by using UC nanoparticles functionalized with biomolecular recognition moieties.[137,141,174] For example, Wang et al.[137] have demonstrated that $NaYF_4$:Yb/Er nanoparticles conjugated with antibody can be used for highly specific staining and imaging of HeLa cells with antigen expressed on the cell membrane. Another representative work has been reported by Zako et al.,[174] who demonstrated the use of Y_2O_3:Er nanoparticles modified with cyclic arginine–glycine–asparatic acid (RGD) peptide for cell imaging studies. They found that these nanoconjugates can specifically bind to cancer cells with elevated integrin $\alpha_v\beta_3$ expression. The ability to non-invasively visualize and monitor integrin $\alpha_v\beta_3$ expression levels will provide new opportunities to document tumor integrin expression, allow appropriate selection of patients for anti-integrin treatment, and evaluate treatment efficacy in integrin-positive patients.

Recently, Jiang et al.[175] have shown that UC nanoparticles can be used for the delivery and tracking of small interference RNA (siRNA). To achieve the target delivery, siRNA were attached to silica-coated $NaYF_4$:Yb/Er nanoparticles modified with anti-Her2 antibody. Intracellular uptake of the nanoparticles was visualized under a confocal microscope and the gene silencing effect of siRNA was evaluated by a luciferase assay. The luciferase assay results showed that the UC nanoparticles can serve as efficient carriers of siRNA for target delivery to specific cells through the attachment of suitable antibodies to the nanoparticles. As an extension of their previous studies on tracking and delivery of siRNA, Jiang and Zhang[176] have demonstrated real-time tracking of the intracellular release of siRNA from UC nanoparticle carriers. To achieve this, they labeled siRNA with BOBO-3 intercalating dye. The measured LRET between the UC nanoparticles and BOBO-3 gives an indication of the siRNA release from the UC nanoparticles.

4.2 In vivo organism and animal imaging

UC particles in vivo staining have made the most progress and attracted the greatest interest. Lim et al.[61] have pioneered the use of UC particles in live organism imaging. In their study, Y_2O_3:Yb/Er nanoparticles in the size range of 50–150 nm were inoculated into live nematode Caenorhabditis elegans (C. elegans) worms and subsequently imaged in the digestive system of the worms. Upon excitation at 980 nm, the statistical distribution of the nanoparticles in the intestines can be clearly visualized (Fig. 14a). Importantly, the nanoparticles have shown good biocompatibility as the worms do not exhibit unusual behavior in feeding. In their most recent work, Lim et al.[66] have refined the synthetic procedure for preparing sub-10-nm Y_2O_3:Yb/Er nanoparticles. The ultra-small nanoparticles hold promise for staining ultra-fine structures in biological systems. However, there is a considerable loss of emission typically associated with ultra-small nanoparticles due to surface quenching.

Recently, the facile preparation of small-sized UC nanoparticles with strong emission intensity and high aqueous dispersity has facilitated the in vivo imaging of small animals by fast intravenous or intradermal injection of nanoparticles.[123,131,177–182] For example, Nyk et al.[179] have
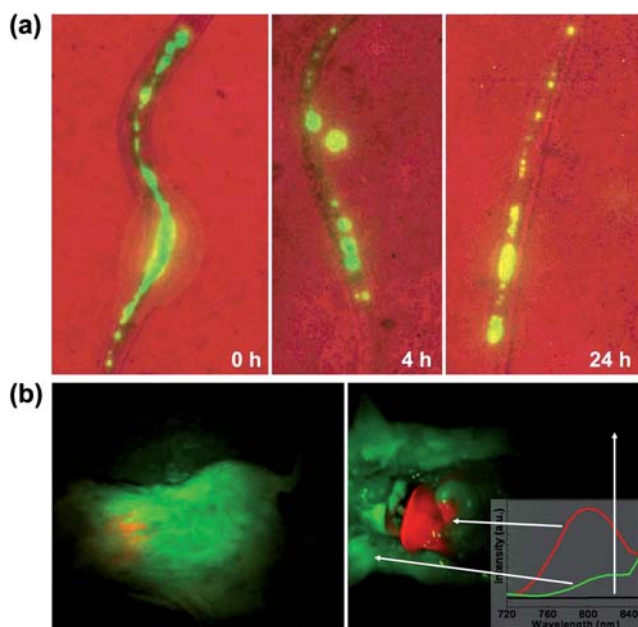
Fig. 14 *In vivo* organism and small animal imaging with UC nano-particles. (a) False color images of *C. elegans* after being deprived of food over various periods of time: the red color represents the brightfield and green for the UC emission. (b) Whole body images of intact mouse (left) and the same mouse after injection with UC nanoparticles and dissection (right): the red color indicates emission from UC nanoparticles and green and black colors show the imaging background; inserted graphics represent the photoluminescence spectra from three different areas as indicated by the arrows. (Reprinted with permission from: (a) ref. 61, and (b) ref. 179. Copyright 2006, 2008, respectively, American Chemical Society.)

demonstrated Maestro whole-body *in vivo* imaging of a Balb-c mouse through use of NIR-to-NIR UC nanoparticles (Fig. 14b). The remarkable advantage offered by this technique is that both the excitation and emission are in the NIR range, allowing imaging of tissue with high penetration depth. Another interesting development has been demonstrated by Hilderbrand *et al.*,[123] who carried out *in vivo* vascular imaging of nude mice using Y_2O_3:Yb/Er nanoparticles coated with PEG polymer. The polymer coating minimizes non-specific tissue binding and prolongs the circulation half-lives of the particles in the blood. Importantly, the UC nanoparticles were found to be sufficiently bright to enable *in situ* imaging during surgery. Recently, real-time imaging based upon UC nanoparticles has been further demonstrated by Kobayashi *et al.*,[131] who showed that the NIR- and green-emitting UC nanoparticles can be used for two-color *in situ* lymphatic imaging without extensive post-image processing.

Conjugated with biomolecular recognition moieties, UC nanoparticles have been used for target imaging *in vivo* for tumor detection and drug delivery. By linking folic acid (FA) and RGD to UC nanoparticles, Xiong *et al.*[119,183] are able to detect HeLa and U87MG tumors inside athymic nude mice. Importantly, region of interest (ROI) analysis of the UC luminescence signal *in vivo* showed that UC imaging achieved a high signal-to-noise ratio (SNR) of *ca.* 24 between the tumor and the background (Fig. 15), which generally cannot be obtained in single-photon or
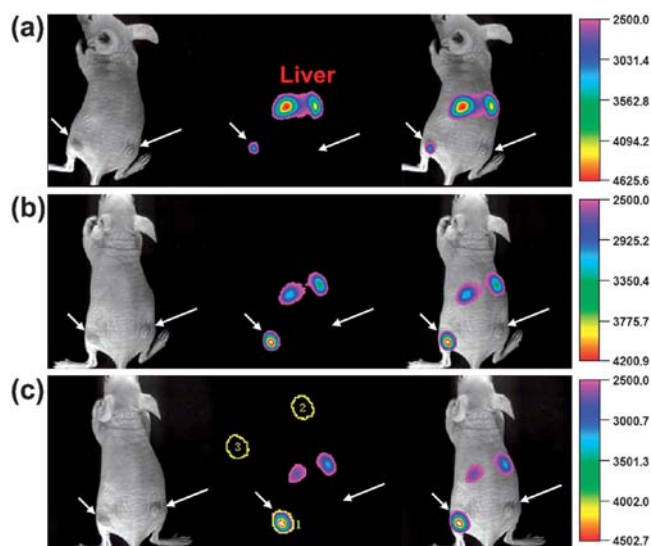

Fig. 15 Target *in vivo* UC luminescence imaging of subcutaneous U87MG tumor (left hind leg, indicated by short arrows) and MCF-7 tumor (right hind leg, indicated by long arrows) borne by athymic nude mice after intravenous injection of RGD-conjugated NaYF₄:Yb/Er/Tm nanoparticles for (a) 1 h, (b) 4 h, and (c) 24 h. The left, middle, and right columns are brightfield, luminescence, and overlay images, respectively. Intense UC luminescence signal was observed in the U87MG tumor whereas no significant signal was seen in the MCF-7 tumor. ROI 1, specific uptake; ROI 2, non-specific uptake; ROI 3, background. *In vivo* SNR = $(I_{ROI\ 1} - I_{ROI\ 3})/(I_{ROI\ 2} - I_{ROI\ 3})$. (Reprinted with permission from ref. 183. Copyright 2009, American Chemical Society.)

two-photon fluorescence imaging.[183] UC particles have also been used for tracking transplanted cells *in vivo*. In a recent work, Idris *et al.*[114] have injected UC nanoparticle-loaded live myoblast cells into a living mouse model of cryoinjured hind limb. *In vivo* confocal imaging was used to study the distribution and activity of the delivered cells.

4.3 Diffuse optical tomography

The term tomography refers to a medical imaging procedure that uses a wave of energy to show cross-sectional images of the samples. Diffuse optical tomography (DOT) is a biomedical imaging technique that utilizes scattered NIR light as a probe for structural variations in tissue. In a typical experiment, a highly-scattering tissue medium is illuminated by a narrow collimated beam and the light which propagates through the medium is collected by an array of detectors attached to the tissue surface. The presence of a tumor or other anomaly inside the tissue can be discerned from the recorded optical data because tumorous tissue has different absorption and scattering properties.

DOT scanning can be achieved through the use of intrinsic contrast agents such as haemoglobin.[184] The sensitivity of detection is further improved by using extrinsic fluorophores such as indocyanine green (ICG).[185,186] To provide high-quality optical data from the DOT scanning, suppression of noise and background tissue autofluorescence is of substantial importance. Although much of the noise can be eliminated by employing low-noise equipment, the tissue autofluorescence remains to plague the measurements with traditional Stokes-shifting fluorophores.
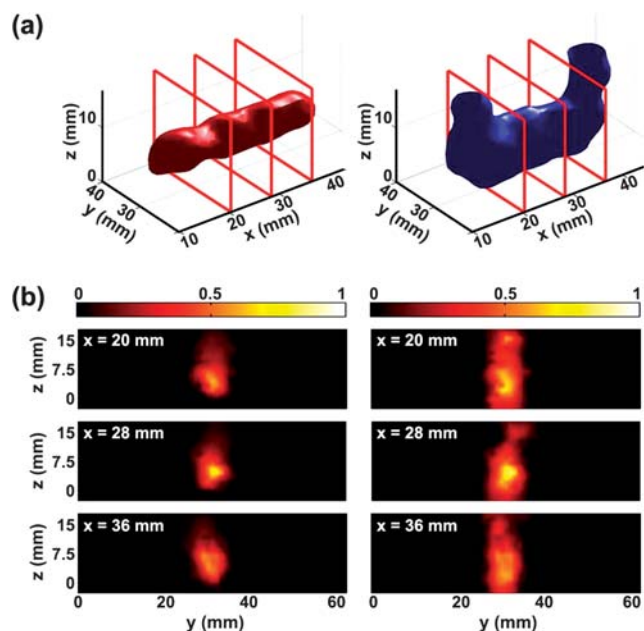
Fig. 16 A comparison of UC nanoparticles (left column) and Rhodamine 6G (right column) in DOT. (a) Three-dimensional rendering of the reconstructed fluorophores: the boxes indicate the position of the cross-sectional slices; reconstruction using UC nanoparticles shows a smooth and uniform rendering, whereas the reconstruction using Rhodamine 6G shows several artifacts. (b) Cross-sectional slices of the reconstructed relative nanoparticle and Rhodamine 6G distributions. (Reprinted with permission from ref. 188. Copyright 2009, American Institute of Physics.)

The ability of UC nanoparticles to emit anti-Stokes-shifted light upon NIR excitation enables the detection of signal in an auto-fluorescence-free environment.[187] Thus, the UC nanoparticles have been suggested as an alternative to fluorophores in DOT. For example, Xu et al.[188] have recently demonstrated the use of NaYF$_4$:Yb/Tm nanoparticles for DOT scanning in a controlled environment by using a gelatin-based tissue phantom. The reconstructed optical data obtained from UC nanoparticles showed a uniform and confined phosphor distribution. In contrast, the reconstructed optical data obtained from the use of an organic fluorophore (Rhodamine 6G) showed severe artifacts at two ends of the fluorescent target (Fig. 16). The results demonstrate that the non-linear power-dependent UC process leads to more sharply defined reconstructions of the phosphor distribution, and also opens the possibility to resolve two closely situated phosphors which cannot be resolved by using fluorophores. A recent study has highlighted another advantage of the use of upconversion nanoparticles in DOT.[189] The study reveals that on account of the non-linear power dependence of the UC process, these nanoparticles can be simultaneously excited by two or more excitation beams, leading to multiple tomographic images. Analysis of these multiple images yields additional information and leads to improved reconstruction of the optical data.

4.4 Multimodal imaging

The basic concept of multimodal imaging lies in the incorporation of two imaging modalities within the setting of a single
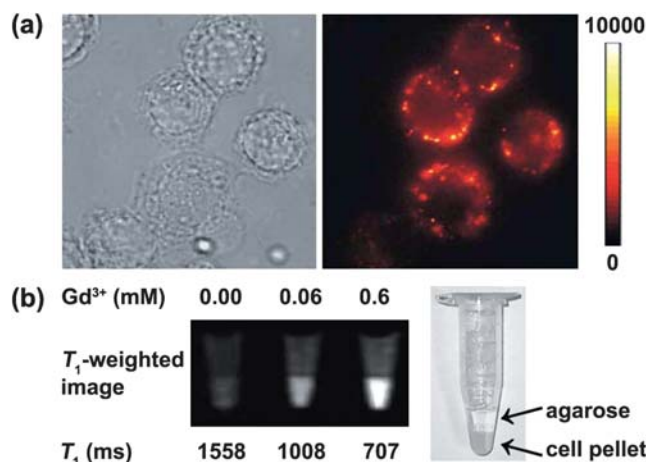

Fig. 17 Multimodal imaging with NaGdF$_4$:Yb/Er nanoparticles. (a) Brightfield (left) and luminescence (right) images of SK-BR-3 cells incubated with the UC nanoparticles at Gd^{3+} concentration of 100 mg/ml for 4 h. (b) T_1-weighted magnetic resonance images of SK-BR-3 cells (1.3×10^7 cells) incubated with the UC nanoparticles at various concentrations for 24 h. (Reprinted with permission from ref. 97. Copyright 2009, Wiley-VCH Verlag GmbH & Co. KGaA.)

examination. UC nanoparticles have been well established as contrast agents for optical spectroscopy. In recent years, attempts have been made to develop multimodal imaging agents based on UC nanoparticles. The multimodal imaging agents are fabricated in accordance with the following two strategies. One such approach involves the incorporation of gadolinium (Gd^{3+}), widely used as the contrast agent in magnetic resonance imaging (MRI),[190,191] in the crystal host lattice to develop particles that can simultaneously serve as optical and magnetic contrast agents. Gd^{3+}-based UC phosphors have been developed as multimodal imaging agents by the groups of Hyeon,[97] Li,[129] Prasad,[192] and Tan.[193] In a representative example, Hyeon and co-workers[97] have demonstrated the use of NaGd$_4$:Yb/Er nanoparticles for optical and magnetic resonance imaging in breast cancer cells (SK-BR-3) (Fig. 17). In a recent study conducted by Li and co-workers,[129] the multimodal imaging via NaGdF$_4$-based nanoparticles has been extended to live animals. Since the luminescent center and the magnetic contrast agent are incorporated in the same host matrix, this approach avoids complicated procedures of combining individual optical and magnetic contrast agents. Another benefit of this approach is a greater level of control over the fabrication of smaller particles as multimodal imaging agents.

The second approach uses the encapsulation of UC nanoparticles in a silica shell followed by impregnation of the shell with other reporter molecules. By using this strategy, Li and co-workers[141] fabricated UC nanoparticles with an organic dye-impregnated silica shell (Fig. 18). Folic acid was attached on the surface of the shell for targeting human cells that over-express tumor markers on a variety of human cancers. They then demonstrated receptor-mediated delivery of FA-conjugated nanocomposites targeting KB cells by using UC luminescence microscopy and downconversion flow cytometry. In a similar way, Zhang and co-workers[194] have demonstrated that Gd-based MRI contrast agents could be incorporated into the silica shells
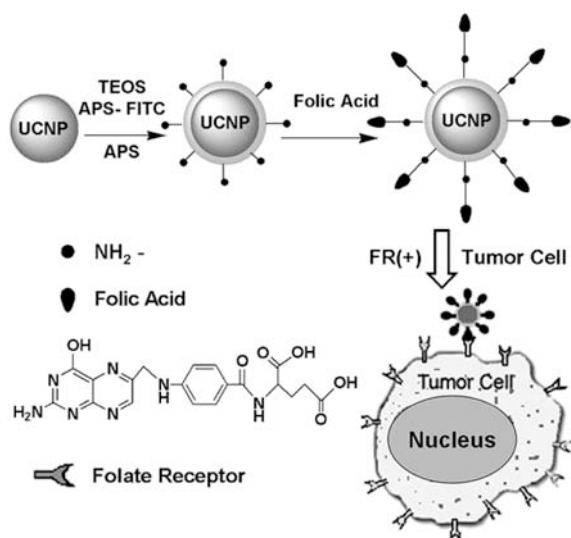
Fig. 18 Schematic of the synthesis of folic acid-functionalized silica-coated NaYF$_4$:Yb/Er nanoparticles and folate-mediated binding of a folate receptor-positive [FR(+)] tumor cells. UCNP: upconversion nanoparticle; TEOS: tetraethylorthosilicate; FITC: fluorescein isothiocyanate; APS: (3-aminopropyl)triethoxysilane. (Reprinted with permission from ref. 141. Copyright 2009, Wiley-VCH Verlag GmbH & Co. KGaA.)

coated on UC nanoparticles, providing an alternative route towards dual-functional contrast agents with optical and magnetic imaging capabilities. Besides amorphous shells, crystalline materials comprising Gd^{3+} ions have also been grown on the UC nanoparticles to endow the nanoparticles with dual-imaging capabilities.[195,196] The spatial confinement of the second

staining agent in the shell can minimize its interaction with the UC core and thus maximize the functionalities of both the core and the shell, despite causing an increase in the particle size.

5. As light transducers for cancer therapy

Since the discovery that cancer cells are vulnerable to certain photosensitive chemicals under red light beams, photodynamic therapy (PDT) has recently emerged as an increasingly effective, non-invasive, economical treatment for cancers and premalignant conditions.[197] In principle, PDT involves three basic steps: (i) selective uptake and localization of a photosensitizer into specific tumor cell/tissue type, (ii) irradiation of the photosensitizer with predetermined intense doses of light to activate the photosensitizer, and (iii) generation of reactive oxygen species (ROS) that kill nearby abnormal cells with little or no effect on the surrounding tissues.

In general, there are three main pathways associated with the killing of cancer cells by PDT.[198] In the first case, the active form of oxygen generated by PDT directly destroys the tumor cells.[199] PDT can also damage blood vessels in the tumor, thus preventing the cancer from receiving the necessary nutrients.[200,201] In addition, PDT may activate the immune system against uncontrollable invasion and damage to normal tissues by tumor cells.[202]

Conventional PDT techniques have proved effective in the treatment of a number of cancers. However, the light needed to activate photosensitizers penetrates only about a centimeter (approximately one-third of an inch) of tissue. In this regard, PDT is most often used to treat tumors on or just beneath the skin's surface, or on the linings of internal organs or cavities. Another limitation of conventional PDT is the ineffectiveness in treating large tumors or metastatic cancers that have spread.

Table 2 Recent progress in the development of UC nanoparticle-based PDT

Photosensitizer[a]	Surface modification	PDT activity	Remarks	Ref.
Merocyanine 540	Porous silica	*In vitro* study on destruction of MCF-7/AZ bladder cancer cells	Low photosensitizer loading. Highly specific delivery to cancer cells. Capable of targeting different types of cancer cells. Reduced ease of diffusion of ROS from a silica shell	204
Zinc phthalocyanine	Polyethylenimine	Quenching of ABDA fluorescence as an indication of singlet oxygen generation	Low photosensitizer loading due to fast desorption of PS from the polyethylenimine coating	205
Tetraphenylporphyrin	Poly(ethylene glycol)	Quenching of ADPA fluorescence as an indication of singlet oxygen generation	High photosensitizer loading and improved biocompatible coating	206
Zinc phthalocyanine	Mesoporous silica	Quenching of ABDA fluorescence as an indication of singlet oxygen generation, reduced cell viability of murine bladder cancer cells	Low photosensitizer loading. Improved diffusion of ROS due to the mesoporous shell structure. Recyclable use of the nanoparticles after removal of the shell in ethanol	207
Zinc phthalocyanine	Mesoporous silica	Green fluorescence from oxidized fluorescein derivative in live cells as an indication of singlet oxygen generation. Reduced cell viability, condensation of nuclear chromatin, internucleosomal DNA fragmentation, release of *cytochrome c* from mitochondria and an inability to express specific proteins in murine bladder cancer cells as an indication of cell damage.	Low photosensitizer loading. Improved diffusion of ROS through mesoporous shells, recyclable use of nanoparticles. Demonstration of singlet oxygen generation *in vitro*. Mechanistic insight into the cell damage induced by singlet oxygen produced as a result of irradiation of nanoparticles with NIR	208

[a] The photosensitizers in the list are immobilized on NaYF$_4$:Yb/Er nanoparticles followed by surface modification with a silica or polymer layer.

Researchers are investigating ways to improve equipment and delivery of the activating light through use of fiber-optic tubes and magnetic nanoparticles.[203]

The development of UC nanoparticles capable of converting NIR light into the visible range has attracted considerable recent interest in PDT because NIR radiation penetrates deep into biological tissues.[204–208] The upconverted visible emission from the nanoparticles can excite photosensitizers and subsequently generate ROS.[209] The use of UC nanoparticles with tunable emissions provides an additional benefit to excite specific sensitizers. In addition, the nanoparticles provide a convenient platform for photosensitizer coupling, magnetic coatings, and cancer-cell targeting.

Table 2 summarizes recent works on the application of UC nanoparticles in PDT. In most of these studies, the UC nanoparticles are pre-modified with a shell impregnated with photosensitizers to generate composite nanomaterials (Fig. 19). The shell also stabilizes the nanoparticles in aqueous solutions and provides the ability to target a specific cancer cell. $NaYF_4$:Yb/Er nanoparticles are primarily used due to their high efficiency of UC, while a wide variety of photosensitizers including porphyrins, merocyanine 540 and zinc phthalocyanides are used.

Zhang *et al.*[204] first demonstrated the application of UC nanoparticle-based PDT in MCF-7/AZ bladder cancer cells. To establish the effect of UC nanoparticle-based PDT on cell viability, the photosensitizer-impregnated nanoparticles were modified with mouse monoclonal antibodies that specifically bind to the cancer cells. The antibody-modified nanoparticles were then loaded into the cancer cells. Upon NIR irradiation, cell death was observed within 1 h of incubation. To further improve the therapeutic efficiency, the challenge is to achieve a coating of photosensitizers on UC nanoparticles at high concentrations. Austin and co-workers[206] have been successful to boost the nanoparticle-to-photosensitizer ratio to 3:1. On NIR irradiation, the photosensitizer-loaded UC nanoparticles generate singlet oxygen, which is detected through the quenching of fluorescence of 9,10-anthracenedipropionic acid (ADPA). In an attempt to assist the release of the singlet oxygen from the photosensitizer-impregnated nanoparticles, Zhang and co-workers[207] have used a mesoporous silica coating on the UC nanoparticles. The effectiveness of the nanoparticles for the therapeutic action has been tested both by the fluorescence quenching of 9,10-anthracenediyl-bis(methylene)dimalonic acid (ABDA) and reduced cell viability of cancerous cells. More recently, this group have extended their studies to mechanistic investigation of nanoparticle-based PDT in murine bladder cancer cells.[208] They have demonstrated the detection of singlet oxygen *in vitro* by the observation of recovered green fluorescence from a fluorescein derivative upon oxidation. The PDT activity was monitored through an array of analytical techniques such as cell viability tests, protein release and expression assays, and gel electrophoresis analysis. The results indicate that cell damage in nanoparticle-based PDT is associated with chromatin condensation in the nucleus and fragmentation of nucleosomal DNA. In addition, the damaged cells showed mitochondrial failure which resulted in the release of the mitochondrial protein *cytochrome c* into the cell cytoplasm. The damage to cancerous cells was also monitored through the expression of the PSA in carcinoma transfectant cell line MB49-PSA cells. This cell line expresses the PSA protein as a tumor marker. When incubated with photosensitizer-modified UC nanoparticles, the cells showed a marked reduction in the PSA protein expression, which is indicative of cell damage. Importantly, it should be noted that the main objective in the fabrication of nanoparticle-based PDT agents is to achieve improved therapeutic effects in live organisms. However, there has been no report demonstrating *in vivo* application of photosensitizer-modified UC nanoparticles as PDT agents.

6. Conclusions

In this review, the principles and recent technological advances in biological applications of luminescent UC nanoparticles have been discussed. These methods are emerging as valuable tools that enable ultra-sensitive molecular detection without photodamage of the molecules and visualization of cellular features with substantial depth of penetration.

In addition to providing useful luminescent biolabels with high photostability, UC nanoparticles have shown promising results when used in PDT for the treatment of cancer. To fully realize the potential of this technique, we need to develop innovative strategies to couple photosensitizers to the nanoparticles with high loading efficiency and without significantly increasing the particle size. Further development of smaller and brighter UC nanoparticles with tunable emission colors,[210,211] combined with improvements in the detection technology and imaging equipment, will consolidate the position of UC nanoparticle labeling technology as a versatile approach to addressing some of today's most challenging problems.
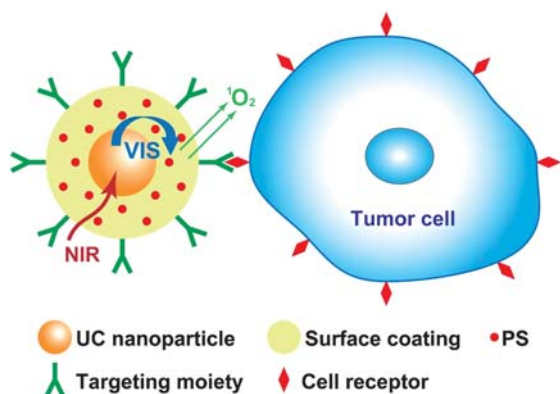

Fig. 19 Schematic design of UC nanoparticle-based PDT for the treatment of a tumor cell. The design is composed of a nanoparticle core and a porous silica or polymer shell impregnated with photosensitizers. The shell is also modified with functional groups for targeting a specific tumor cell.

References

1 F. Wang, W. B. Tan, Y. Zhang, X. P. Fan and M. Q. Wang, *Nanotechnology*, 2006, **17**, R1–R13.

2 M. Bruchez Jr., M. Moronne, P. Gin, S. Weiss and A. P. Alivisatos, *Science*, 1998, **281**, 2013–2016.

3 W. C. W. Chan and S. M. Nie, *Science*, 1998, **281**, 2016–2018.

4 J. K. Jaiswal, H. Mattoussi, J. M. Mauro and S. M. Simon, *Nat. Biotechnol.*, 2003, **21**, 47–51.

5 X. Michalet, F. F. Pinaud, L. A. Bentolila, J. M. Tsay, S. Doose, J. J. Li, G. Sundaresan, A. M. Wu, S. S. Gambhir and S. Weiss, *Science*, 2005, **307**, 538–544.

6 I. L. Medintz, H. T. Uyeda, E. R. Goldman and H. Mattoussi, *Nat. Mater.*, 2005, **4**, 435–446.

7 T. Jamieson, R. Bakhshi, D. Petrova, R. Pocock, M. Imani and A. M. Seifalian, *Biomaterials*, 2007, **28**, 4717–4732.

8 J. K. Jaiswal and S. M. Simon, *Trends Cell Biol.*, 2004, **14**, 497–504.

9 A. M. Derfus, W. C. W. Chan and S. N. Bhatia, *Nano Lett.*, 2004, **4**, 11–18.

10 M. Nirmal, B. O. Dabbousi, M. G. Bawendi, J. J. Macklin, J. K. Trautman, T. D. Harris and L. E. Brus, *Nature*, 1996, **383**, 802–804.

11 W. M. Yen and M. J. Weber, *Inorganic phosphors: compositions, preparation and optical properties*, CRC Press, Florida, 2004.

12 G. Blasse and B. C. Grabmaier, *Luminescent Materials*, Springer, Berlin, 1994.

13 K. Riwotzki, H. Meyssamy, H. Schnablegger, A. Kornowski and M. Haase, *Angew. Chem., Int. Ed.*, 2001, **40**, 573–576.

14 J. W. Stouwdam, M. Raudsepp and F. van Veggel, *Langmuir*, 2005, **21**, 7003–7008.

15 F. Wang, Y. Zhang, X. P. Fan and M. Q. Wang, *J. Mater. Chem.*, 2006, **16**, 1031–1034.

16 K. Binnemans, *Chem. Rev.*, 2009, **109**, 4283–4374.

17 S. V. Eliseeva and J. C. G. Bunzli, *Chem. Soc. Rev.*, 2010, **39**, 189–227.

18 H. Goesmann and C. Feldmann, *Angew. Chem., Int. Ed.*, 2010, **49**, 1362–1395.

19 E. Beaurepaire, V. Buissette, M. P. Sauviat, D. Giaume, K. Lahlil, A. Mercuri, D. Casanova, A. Huignard, J. L. Martin, T. Gacoin, J. P. Boilot and A. Alexandrou, *Nano Lett.*, 2004, **4**, 2079–2083.

20 F. Meiser, C. Cortez and F. Caruso, *Angew. Chem., Int. Ed.*, 2004, **43**, 5954–5957.

21 D. Casanova, D. Giaume, M. Moreau, J. L. Martin, T. Gacoin, J. P. Boilot and A. Alexandrou, *J. Am. Chem. Soc.*, 2007, **129**, 12592–12593.

22 J. Q. Gu, J. Shen, L. D. Sun and C. H. Yan, *J. Phys. Chem. C*, 2008, **112**, 6589–6593.

23 J. Shen, L. D. Sun and C. H. Yan, *Dalton Trans.*, 2008, 5687–5697.

24 K. L. Wong, G. L. Law, M. B. Murphy, P. A. Tanner, W. T. Wong, P. K. S. Lam and M. H. W. Lam, *Inorg. Chem.*, 2008, **47**, 5190–5196.

25 C. A. Traina, T. J. Dennes and J. Schwartz, *Bioconjugate Chem.*, 2009, **20**, 437–439.

26 G. F. J. Garlick, in *Handbuch der Physik*, ed. S. Flügge, Springer, Berlin, 1958, **26**, 1.

27 S. Sivakumar, F. van Veggel and P. S. May, *J. Am. Chem. Soc.*, 2007, **129**, 620–625.

28 F. Auzel, *Chem. Rev.*, 2004, **104**, 139–173.

29 J. F. Suyver, A. Aebischer, D. Biner, P. Gerner, J. Grimm, S. Heer, K. W. Krämer, C. Reinhard and H. U. Güdel, *Opt. Mater.*, 2005, **27**, 1111–1130.

30 F. Wang and X. G. Liu, *Chem. Soc. Rev.*, 2009, **38**, 976–989.

31 C. Jiang and W. B. Xu, *J. Disp. Technol.*, 2009, **5**, 312–318.

32 S. Heer, O. Lehmann, M. Haase and H. U. Güdel, *Angew. Chem., Int. Ed.*, 2003, **42**, 3179–3182.

33 S. Heer, K. Kömpe, H. U. Güdel and M. Haase, *Adv. Mater.*, 2004, **16**, 2102–2105.

34 A. Patra, C. S. Friend, R. Kapoor and P. N. Prasad, *Appl. Phys. Lett.*, 2003, **83**, 284–286.

35 G. S. Yi, H. C. Lu, S. Y. Zhao, G. Yue, W. J. Yang, D. P. Chen and L. H. Guo, *Nano Lett.*, 2004, **4**, 2191–2196.

36 K. W. Krämer, D. Biner, G. Frei, H. U. Güdel, M. P. Hehlen and S. R. Lüthi, *Chem. Mater.*, 2004, **16**, 1244–1251.

37 G. F. Wang, W. P. Qin, J. S. Zhang, Y. Wang, C. Y. Cao, L. L. Wang, G. D. Wei, P. F. Zhu and R. J. Kim, *J. Phys. Chem. C*, 2008, **112**, 12161–12167.

38 D. Q. Chen, Y. S. Wang, K. L. Zheng, T. L. Guo, Y. L. Yu and P. Huang, *Appl. Phys. Lett.*, 2007, **91**, 051920.

39 G. S. Yi, W. B. Lee and G. M. Chow, *J. Nanosci. Nanotechnol.*, 2007, **7**, 2790–2794.

40 H. Schäfer, P. Ptacek, O. Zerzouf and M. Haase, *Adv. Funct. Mater.*, 2008, **18**, 2913–2918.

41 V. Mahalingam, F. Vetrone, R. Naccache, A. Speghini and J. A. Capobianco, *Adv. Mater.*, 2009, **21**, 4025–4028.

42 Y. J. Sun, H. J. Liu, X. Wang, X. G. Kong and H. Zhang, *Chem. Mater.*, 2006, **18**, 2726–2732.

43 M. Liu, S. W. Wang, J. Zhang, L. Q. An and L. D. Chen, *Opt. Mater.*, 2007, **30**, 370–374.

44 C. Feldmann, M. Roming and K. Trampert, *Small*, 2006, **2**, 1248–1250.

45 Z. W. Quan, D. M. Yang, P. P. Yang, X. M. Zhang, H. Z. Lian, X. M. Liu and J. Lin, *Inorg. Chem.*, 2008, **47**, 9509–9517.

46 G. F. Wang, Q. Peng and Y. D. Li, *J. Am. Chem. Soc.*, 2009, **131**, 14200–14201.

47 Z. W. Quan, P. P. Yang, C. X. Li, J. Yang, D. M. Yang, Y. Jin, H. Z. Lian, H. Y. Li and J. Lin, *J. Phys. Chem. C*, 2009, **113**, 4018–4025.

48 G. Y. Chen, Y. G. Zhang, G. Somesfalean, Z. G. Zhang, Q. Sun and F. P. Wang, *Appl. Phys. Lett.*, 2006, **89**, 163105.

49 A. Patra, C. S. Friend, R. Kapoor and P. N. Prasad, *Chem. Mater.*, 2003, **15**, 3650–3655.

50 M. Y. Xie, X. N. Peng, X. F. Fu, J. J. Zhang, G. L. Lia and X. F. Yu, *Scr. Mater.*, 2009, **60**, 190–193.

51 J. H. Zeng, T. Xie, Z. H. Li and Y. D. Li, *Cryst. Growth Des.*, 2007, **7**, 2774–2777.

52 Q. L. Dai, H. W. Song, X. G. Ren, S. Z. Lu, G. H. Pan, X. Bai, B. Dong, R. F. Qin, X. S. Qu and H. Zhang, *J. Phys. Chem. C*, 2008, **112**, 19694–19698.

53 F. Wang, X. P. Fan, D. B. Pi, Z. Y. Wang and M. Q. Wang, *J. Solid State Chem.*, 2005, **178**, 825–830.

54 W. Q. Luo, R. F. Li and X. Y. Chen, *J. Phys. Chem. C*, 2009, **113**, 8772–8777.

55 H. T. Wong, H. L. W. Chan and J. H. Hao, *Appl. Phys. Lett.*, 2009, **95**, 022512.

56 C. L. Jiang, F. Wang, N. Q. Wu and X. G. Liu, *Adv. Mater.*, 2008, **20**, 4826–4829.

57 H. Schäfer, P. Ptacek, H. Eickmeier and A. Haase, *J. Nanomater.*, 2009, **2009**, 685624.

58 C. Lorbeer, J. Cybinska and A. V. Mudring, *Chem. Commun.*, 2010, **46**, 571–573.

59 F. Wang, X. P. Fan, D. P. Pi and M. Q. Wang, *Solid State Commun.*, 2005, **133**, 775–779.

60 Y. S. Liu, D. T. Tu, H. M. Zhu, R. F. Li, W. Q. Luo and X. Y. Chen, *Adv. Mater.*, 2010, **22**, DOI: 10.1002/adma.201000128.

61 S. F. Lim, R. Riehn, W. S. Ryu, N. Khanarian, C. K. Tung, D. Tank and R. H. Austin, *Nano Lett.*, 2006, **6**, 169–174.

62 H. Z. Wang, M. Uehara, H. Nakamura, M. Miyazaki and H. Maeda, *Adv. Mater.*, 2005, **17**, 2506–2509.

63 A. M. Pires, O. A. Serra and M. R. Davolos, *J. Lumin.*, 2005, **113**, 174–182.

64 G. K. Das and T. T. Y. Tan, *J. Phys. Chem. C*, 2008, **112**, 11211–11217.

65 F. Vetrone, J. C. Boyer, J. A. Capobianco, A. Speghini and M. Bettinelli, *J. Appl. Phys.*, 2004, **96**, 661–667.

66 S. F. Lim, R. Riehn, C. K. Tung, W. S. Ryu, R. Zhuo, J. Dalland and R. H. Austin, *Nanotechnology*, 2009, **20**, 405701.

67 F van de Rijke, H. Zijlmans, S. Li, T. Vail, A. K. Raap, R. S. Niedbala and H. J. Tanke, *Nat. Biotechnol.*, 2001, **19**, 273–276.

68 X. X. Luo and W. H. Cao, *J. Alloys Compd.*, 2008, **460**, 529–534.

69 S. Sivakumar, P. R. Diamente and F. C. van Veggel, *Chem.–Eur. J.*, 2006, **12**, 5878–5884.

70 G. S. Yi and G. M. Chow, *J. Mater. Chem.*, 2005, **15**, 4460–4464.

71 G. J. H. De, W. P. Qin, J. S. Zhang and D. Zhao, *Chem. Lett.*, 2005, **34**, 914–915.
72 C. H. Liu and D. P. Chen, *J. Mater. Chem.*, 2007, **17**, 3875–3880.
73 Y. W. Zhang, X. Sun, R. Si, L. P. You and C. H. Yan, *J. Am. Chem. Soc.*, 2005, **127**, 3260–3261.
74 C. H. Liu, J. Sun, H. Wang and D. P. Chen, *Scr. Mater.*, 2008, **58**, 89–92.
75 Z. Q. Li, Y. Zhang and S. Jiang, *Adv. Mater.*, 2008, **20**, 4765–4769.
76 Z. Q. Li and Y. Zhang, *Angew. Chem., Int. Ed.*, 2006, **45**, 7732–7735.
77 J. H. Zeng, J. Su, Z. H. Li, R. X. Yan and Y. D. Li, *Adv. Mater.*, 2005, **17**, 2119–2123.
78 F. Wang, D. K. Chatterjee, Z. Q. Li, Y. Zhang, X. P. Fan and M. Q. Wang, *Nanotechnology*, 2006, **17**, 5786–5791.
79 L. Y. Wang and Y. D. Li, *Chem. Mater.*, 2007, **19**, 727–734.
80 F. Zhang, Y. Wan, T. Yu, F. Q. Zhang, Y. F. Shi, S. H. Xie, Y. G. Li, L. Xu, B. Tu and D. Y. Zhao, *Angew. Chem., Int. Ed.*, 2007, **46**, 7976–7979.
81 Y. Wei, F. Q. Lu, X. R. Zhang and D. P. Chen, *J. Alloys Compd.*, 2008, **455**, 376–384.
82 H. X. Mai, Y. W. Zhang, R. Si, Z. G. Yan, L. D. Sun, L. P. You and C. H. Yan, *J. Am. Chem. Soc.*, 2006, **128**, 6426–6436.
83 J. C. Boyer, F. Vetrone, L. A. Cuccia and J. A. Capobianco, *J. Am. Chem. Soc.*, 2006, **128**, 7444–7445.
84 G. S. Yi and G. M. Chow, *Adv. Funct. Mater.*, 2006, **16**, 2324–2329.
85 J. N. Shan and Y. G. Ju, *Appl. Phys. Lett.*, 2007, **91**, 123103.
86 C. H. Liu, H. Wang, X. Li and D. P. Chen, *J. Mater. Chem.*, 2009, **19**, 3546–3553.
87 M. Wang, J. L. Liu, Y. X. Zhang, W. Hou, X. L. Wu and S. K. Xu, *Mater. Lett.*, 2009, **63**, 325–327.
88 X. M. Liu, J. W. Zhao, Y. J. Sun, K. Song, Y. Yu, C. A. Du, X. G. Kong and H. Zhang, *Chem. Commun.*, 2009, 6628–6630.
89 C. Zhang and J. Chen, *Chem. Commun.*, 2010, **46**, 592–594.
90 C. Chen, L. D. Sun, Z. X. Li, L. L. Li, J. Zhang, Y. W. Zhang and C. H. Yan, *Langmuir*, 2010, DOI: 10.1021/la904545a.
91 X. Chen, W. J. Wang, X. Y. Chen, J. H. Bi, L. Wu, Z. H. Li and X. Z. Fu, *Mater. Lett.*, 2009, **63**, 1023–1026.
92 L. Zhang and Y. J. Zhu, *J. Inorg. Mater.*, 2009, **24**, 553–558.
93 H. Q. Wang and T. Nann, *ACS Nano*, 2009, **3**, 3804–3808.
94 A. Aebischer, S. Heer, D. Biner, K. Krämer, M. Haase and H. U. Güdel, *Chem. Phys. Lett.*, 2005, **407**, 124–128.
95 F. Wang, X. P. Fan, M. Q. Wang and Y. Zhang, *Nanotechnology*, 2007, **18**, 025701.
96 R. Naccache, F. Vetrone, V. Mahalingam, L. A. Cuccia and J. A. Capobianco, *Chem. Mater.*, 2009, **21**, 717–723.
97 Y. I. Park, J. H. Kim, K. T. Lee, K.-S. Jeon, H. B. Na, J. H. Yu, H. M. Kin, N. Lee, S. H. Choi, S.-I. Baik, H. Kin, S. P. Park, B.-J. Park, Y. W. Kim, S. H. Lee, S.-Y. Yoon, I. C. Song, W. K. Moon, Y. D. Suh and T. Hyeon, *Adv. Mater.*, 2009, **21**, 4467–4471.
98 C. H. Liu, H. Wang, X. R. Zhang and D. P. Chen, *J. Mater. Chem.*, 2009, **19**, 489–496.
99 F. Vetrone and J. A. Capobianco, *Int. J. Nanotechnol.*, 2008, **5**, 1306–1339.
100 Z. G. Yan and C. H. Yan, *J. Mater. Chem.*, 2008, **18**, 5046–5059.
101 P. Rahman and M. Green, *Nanoscale*, 2009, **1**, 214–224.
102 F. Wang, Y. Han, C. S. Lim, Y. H. Lu, J. Wang, J. Xu, H. Chen, C. Zhang, M. Hong and X. Liu, *Nature*, 2010, **463**, 1061–1065.
103 X. F. Yu, M. Li, M. Y. Xie, L. D. Chen, Y. Li and Q. Q. Wang, *Nano Res.*, 2010, **3**, 51–60.
104 G. Y. Chen, Y. Liu, Y. G. Zhang, G. Somesfalean, Z. G. Zhang, Q. Sun and F. P. Wang, *Appl. Phys. Lett.*, 2007, **91**, 133103.
105 F. Wang and X. G. Liu, *J. Am. Chem. Soc.*, 2008, **130**, 5642–5643.
106 V. Mahalingam, F. Mangiarini, F. Vetrone, V. Venkatramu, M. Bettinelli, A. Speghini and J. A. Capobianco, *J. Phys. Chem. C*, 2008, **112**, 17745–17749.
107 B. Dong, H. W. Song, R. F. Qin, X. Bai, S. Z. Lu, X. G. Ren, G. H. Pan, H. Zhang, F. Wang and L. B. Fan, *J. Nanosci. Nanotechnol.*, 2008, **8**, 3921–3925.
108 J. Yang, C. M. Zhang, C. Peng, C. X. Li, L. L. Wang, R. T. Chai and J. Lin, *Chem.–Eur. J.*, 2009, **15**, 4649–4655.
109 L. W. Yang, H. L. Han, Y. Y. Zhang and J. X. Zhong, *J. Phys. Chem. C*, 2009, **113**, 18995–18999.
110 F. Wang, J. Wang, J. Xu, X. J. Xue and X. G. Liu, *Spectrosc. Lett.*, 2010, in press.
111 J. Wang, F. Wang, J. Xu, Y. Liu, H. Chen, X. Chen and X. Liu, *C. R. Chim.*, 2010, **13**, DOI: 10.1016/j.crci.2010.03.021.
112 F. Wang, X. J. Xue and X. G. Liu, *Angew. Chem., Int. Ed.*, 2008, **47**, 906–909.
113 M. X. Yu, F. Y. Li, Z. G. Chen, H. Hu, C. Zhan, H. Yang and C. H. Huang, *Anal. Chem.*, 2009, **81**, 930–935.
114 N. M. Idris, Z. Q. Li, L. Ye, E. K. W. Sim, R. Mahendran, P. C. L. Ho and Y. Zhang, *Biomaterials*, 2009, **30**, 5104–5113.
115 M. D. Barnes, A. Mehta, T. Thundat, R. N. Bhargava, V. Chhabra and B. Kulkarni, *J. Phys. Chem. B*, 2000, **104**, 6099–6102.
116 S. W. Wu, G. Han, D. J. Milliron, S. Aloni, V. Altoe, D. V. Talapin, B. E. Cohen and P. J. Schuck, *Proc. Natl. Acad. Sci. U. S. A.*, 2009, **106**, 10917–10921.
117 P. R. Diamente and F. C. J. M. van Veggel, *J. Fluoresc.*, 2005, **15**, 543–551.
118 F. Wang, Y. Zhang, X. P. Fan and M. Q. Wang, *Nanotechnology*, 2006, **17**, 1527–1532.
119 L. Q. Xiong, Z. G. Chen, M. X. Yu, F. Y. Li, C. Liu and C. H. Huang, *Biomaterials*, 2009, **30**, 5592–5600.
120 Q. B. Zhang, K. Song, J. W. Zhao, X. G. Kong, Y. J. Sun, X. M. Liu, Y. L. Zhang, Q. H. Zeng and H. Zhang, *J. Colloid Interface Sci.*, 2009, **336**, 171–175.
121 T. Y. Cao, T. S. Yang, Y. Cao, Y. Yang, H. Hu and F. Y. Li, *Inorg. Chem. Commun.*, 2010, **13**, 392–394.
122 M. Kamimura, D. Miyamoto, Y. Saito, K. Soga and Y. Nagasaki, *Langmuir*, 2008, **24**, 8864–8870.
123 S. A. Hilderbrand, F. W. Shao, C. Salthouse, U. Mahmood and R. Weissleder, *Chem. Commun.*, 2009, 4188–4190.
124 C. A. Traina and J. Schwartz, *Langmuir*, 2007, **23**, 9158–9161.
125 J. C. Boyer, M. P. Manseau, J. I. Murray and F. C. J. M. van Veggel, *Langmuir*, 2010, **26**, 1157–1164.
126 Z. G. Chen, H. L. Chen, H. Hu, M. X. Yu, F. Y. Li, Q. Zhang, Z. G. Zhou, T. Yi and C. H. Huang, *J. Am. Chem. Soc.*, 2008, **130**, 3023–3029.
127 H. Hu, M. X. Yu, F. Y. Li, Z. G. Chen, X. Gao, L. Q. Xiong and C. H. Huang, *Chem. Mater.*, 2008, **20**, 7003–7009.
128 H. P. Zhou, C. H. Xu, W. Sun and C. H. Yan, *Adv. Funct. Mater.*, 2009, **19**, 3892–3900.
129 J. Zhou, Y. Sun, X. Du, L. Xiong, H. Hu and F. Li, *Biomaterials*, 2010, **31**, 3287–3295.
130 G. S. Yi and G. M. Chow, *Chem. Mater.*, 2007, **19**, 341–343.
131 H. Kobayashi, N. Kosaka, M. Ogawa, N. Y. Morgan, P. D. Smith, C. B. Murray, X. C. Ye, J. Collins, G. A. Kumar, H. Bell and P. L. Choyke, *J. Mater. Chem.*, 2009, **19**, 6481–6484.
132 L. Y. Wang, R. X. Yan, Z. Y. Hao, L. Wang, J. H. Zeng, H. Bao, X. Wang, Q. Peng and Y. D. Li, *Angew. Chem., Int. Ed.*, 2005, **44**, 6054–6057.
133 H. S. Qian, Z. Q. Li and Y. Zhang, *Nanotechnology*, 2008, **19**, 255601.
134 H. C. Lu, G. S. Yi, S. Y. Zhao, D. P. Chen, L. H. Guo and J. Cheng, *J. Mater. Chem.*, 2004, **14**, 1336–1341.
135 Z. Y. Liu, G. S. Yi, H. T. Zhang, J. Ding, Y. W. Zhang and J. M. Xue, *Chem. Commun.*, 2008, 694–696.
136 O. Ehlert, R. Thomann, M. Darbandi and T. Nann, *ACS Nano*, 2008, **2**, 120–124.
137 M. Wang, C. C. Mi, W. X. Wang, C. H. Liu, Y. F. Wu, Z. R. Xu, C. B. Mao and S. K. Xu, *ACS Nano*, 2009, **3**, 1580–1586.
138 S. L. Gai, P. P. Yang, C. X. Li, W. X. Wang, Y. L. Dai, N. Niu and J. Lin, *Adv. Funct. Mater.*, 2010, **20**, 1166–1172.
139 N. J. J. Johnson, N. M. Sangeetha, J. C. Boyer and F. C. J. M. van Veggel, *Nanoscale*, 2010, **2**, 771–777.
140 J. N. Shan, J. B. Chen, J. Meng, J. Collins, W. Soboyejo, J. S. Friedberg and Y. G. Ju, *J. Appl. Phys.*, 2008, **104**, 094308.
141 H. Hu, L. Q. Xiong, J. Zhou, F. Y. Li, T. Y. Cao and C. H. Huang, *Chem.–Eur. J.*, 2009, **15**, 3577–3584.
142 R. A. Jalil and Y. Zhang, *Biomaterials*, 2008, **29**, 4122–4128.
143 G. K. Das, P. P. Y. Chan, A. Teo, J. S. C. Loo, J. M. Anderson and T. T. Y. Tan, *J. Biomed. Mater. Res., Part A*, 2009, **93**, 337–346.
144 J. Hampl, M. Hall, N. A. Mufti, Y. M. M. Yao, D. B. MacQueen, W. H. Wright and D. E. Cooper, *Anal. Biochem.*, 2001, **288**, 176–187.
145 R. S. Niedbala, H. Feindt, K. Kardos, T. Vail, J. Burton, B. Bielska, S. Li, D. Milunic, P. Bourdelle and R. Vallejo, *Anal. Biochem.*, 2001, **293**, 22–30.

146 P. Corstjens, L. van Lieshout, M. Zuiderwijk, D. Kornelis, H. J. Tanke, A. M. Deelder and G. J. van Dam, *J. Clin. Microbiol.*, 2008, **46**, 171–176.

147 J. J. Li, A. L. Ouellette, L. Giovangrandi, D. E. Cooper, A. J. Ricco and G. T. A. Kovacs, *IEEE Trans. Biomed. Eng.*, 2008, **55**, 1560–1571.

148 L. H. Huang, L. Zhou, Y. B. Zhang, C. K. Xie, J. F. Qu, A. J. Zeng, H. J. Huang, R. F. Yang and X. Z. Wang, *IEEE Sens. J.*, 2009, **9**, 1185–1191.

149 P. Corstjens, M. Zuiderwijk, A. Brink, S. Li, H. Feindt, R. S. Neidbala and H. Tanke, *Clin. Chem.*, 2001, **47**, 1885–1893.

150 M. Zuiderwijk, H. J. Tanke, R. S. Niedbala and P. Corstjens, *Clin. Biochem.*, 2003, **36**, 401–403.

151 P. L. A. M. Corstjens, S. Li, M. Zuiderwijk, K. Kardos, W. R. Abrams, R. S. Niedbala and H. J. Tanke, *IEE Proc.: Nanobiotechnol.*, 2005, **152**, 64–72.

152 T. Ukonaho, T. Rantanen, L. Jamsen, K. Kuningas, H. Pakkila, T. Lovgren and T. Soukka, *Anal. Chim. Acta*, 2007, **596**, 106–115.

153 L. Y. Wang and Y. D. Li, *Chem. Commun.*, 2006, 2557–2559.

154 T. Soukka, T. Rantanen and K. Kuningas, *Ann. N. Y. Acad. Sci.*, 2008, **1130**, 188–200.

155 P. R. Selvin, T. M. Rana and J. E. Hearst, *J. Am. Chem. Soc.*, 1994, **116**, 6029–6030.

156 P. R. Selvin, *Annu. Rev. Biophys. Biomol. Struct.*, 2002, **31**, 275–302.

157 C. G. Morgan and A. C. Mitchell, *Biosens. Bioelectron.*, 2007, **22**, 1769–1775.

158 K. Kuningas, T. Rantanen, T. Ukonaho, T. Lovgren and T. Soukka, *Anal. Chem.*, 2005, **77**, 7348–7355.

159 T. Rantanen, M.-L. Järvenpää, J. Vuojola, R. Arppe, K. Kuningas and T. Soukka, *Analyst*, 2009, **134**, 1713–1716.

160 K. Kuningas, T. Ukonaho, H. Pakkila, T. Rantanen, J. Rosenberg, T. Lovgren and T. Soukka, *Anal. Chem.*, 2006, **78**, 4690–4696.

161 K. Kuningas, H. Pakkila, T. Ukonaho, T. Rantanen, T. Lovgren and T. Soukka, *Clin. Chem.*, 2007, **53**, 145–146.

162 T. Rantanen, H. Pakkila, L. Jamsen, K. Kuningas, T. Ukonaho, T. Lovgren and T. Soukka, *Anal. Chem.*, 2007, **79**, 6312–6318.

163 P. Zhang, S. Rogelj, K. Nguyen and D. Wheeler, *J. Am. Chem. Soc.*, 2006, **128**, 12410–12411.

164 M. Kumar, Y. Guo and P. Zhang, *Biosens. Bioelectron.*, 2009, **24**, 1522–1526.

165 M. Kumar and P. Zhang, *Langmuir*, 2009, **25**, 6024–6027.

166 M. Wang, W. Hou, C. C. Mi, W. X. Wang, Z. R. Xu, H. H. Teng, C. B. Mao and S. K. Xu, *Anal. Chem.*, 2009, **81**, 8783–8789.

167 T. Rantanen, M. L. Jarvenpaa, J. Vuojola, K. Kuningas and T. Soukka, *Angew. Chem., Int. Ed.*, 2008, **47**, 3811–3813.

168 K. König, *J. Microsc.*, 2000, **200**, 83–104.

169 W. Denk, J. H. Strickler and W. W. Webb, *Science*, 1990, **248**, 73–76.

170 D. R. Larson, W. R. Zipfel, R. M. Williams, S. W. Clark, M. P. Bruchez, F. W. Wise and W. W. Webb, *Science*, 2003, **300**, 1434–1436.

171 H. Zijlmans, J. Bonnet, J. Burton, K. Kardos, T. Vail, R. S. Niedbala and H. J. Tanke, *Anal. Biochem.*, 1999, **267**, 30–36.

172 F. Vetrone, R. Naccache, A. J. de la Fuente, F. Sanz-Rodriguez, A. Blazquez-Castro, E. M. Rodriguez, D. Jaque, J. G. Sole and J. A. Capobianco, *Nanoscale*, 2010, **2**, 495–498.

173 L. Yu, Y. Lu, N. Man, S.-H. Yu and L.-P. Wen, *Small*, 2009, **5**, 2784–2787.

174 T. Zako, H. Nagata, N. Terada, A. Utsumi, M. Sakono, M. Yohda, H. Ueda, K. Soga and M. Maeda, *Biochem. Biophys. Res. Commun.*, 2009, **381**, 54–58.

175 S. Jiang, Y. Zhang, K. M. Lim, E. K. W. Sim and L. Ye, *Nanotechnology*, 2009, **20**, 155101.

176 S. Jiang and Y. Zhang, *Langmuir*, 2010, **26**, 6689–6694.

177 I. Texier, E. Heinrich, M. Berger, O. Tillement, C. Louis and P. Peltie, in *Genetically Engineered and Optical Probes for Biomedical Applications IV*, ed. S. Achilefu, D. J. Bornhop, R. Raghavachari, A. P. Savitsky and R. M. Wachter, *Proc. SPIE*, 2007, **6449**, 64490D1–64490D11.

178 D. K. Chatterjee, A. J. Rufaihah and Y. Zhang, *Biomaterials*, 2008, **29**, 937–943.

179 M. Nyk, R. Kumar, T. Y. Ohulchanskyy, E. J. Bergey and P. N. Prasad, *Nano Lett.*, 2008, **8**, 3834–3838.

180 C. Salthouse, S. Hildebrand, R. Weissleder and U. Mahmood, *Opt. Express*, 2008, **16**, 21731–21737.

181 C. Vinegoni, D. Razansky, S. A. Hilderbrand, F. W. Shao, V. Ntziachristos and R. Weissleder, *Opt. Lett.*, 2009, **34**, 2566–2568.

182 Z. Tian, G. Y. Chen, X. Li, H. J. Liang, Y. S. Li, Z. G. Zhang and Y. Tian, *Lasers Med. Sci.*, 2010, **25**, 479–484.

183 L. Q. Xiong, Z. G. Chen, Q. W. Tian, T. Y. Cao, C. J. Xu and C. H. Huang, *Anal. Chem.*, 2009, **81**, 8687–8694.

184 B. W. Pogue, S. P. Poplack, T. O. McBride, W. A. Wells, K. S. Osterman, U. L. Osterberg and K. D. Paulsen, *Radiology*, 2001, **218**, 261–266.

185 V. Ntziachristos, A. G. Yodh, M. Schnall and B. Chance, *Proc. Natl. Acad. Sci. U. S. A.*, 2000, **97**, 2767–2772.

186 A. Joshi, W. Bangerth, K. Hwang, J. C. Rasmussen and E. M. Sevick-Muraca, *Med. Phys.*, 2006, **33**, 1299–1310.

187 C. T. Xu, N. Svensson, J. Axelsson, P. Svenmarker, G. Somesfalean, G. Y. Chen, H. J. Liang, H. C. Liu, Z. G. Zhang and S. Andersson-Engels, *Appl. Phys. Lett.*, 2008, **93**, 171103.

188 C. T. Xu, J. Axelsson and S. Andersson-Engels, *Appl. Phys. Lett.*, 2009, **94**, 251107.

189 H. C. Liu, C. T. Xu and S. Andersson-Engels, *Opt. Lett.*, 2010, **35**, 718–720.

190 P. H. Kuo, E. Kanal, A. K. Abu-Alfa and S. E. Cowper, *Radiology*, 2007, **242**, 647–649.

191 P. Caravan, *Chem. Soc. Rev.*, 2006, **35**, 512–523.

192 R. Kumar, M. Nyk, T. Y. Ohulchanskyy, C. A. Flask and P. N. Prasad, *Adv. Funct. Mater.*, 2009, **19**, 853–859.

193 G. K. Das, B. C. Heng, S. C. Ng, T. White, J. S. C. Loo, L. D'Silva, P. Padmanabhan, K. K. Bhakoo, S. T. Selvan and T. T. Y. Tan, *Langmuir*, 2010, DOI: 10.1021/la904751q.

194 Z. Q. Li, Y. Zhang, B. Shuter and N. M. Idris, *Langmuir*, 2009, **25**, 12015–12018.

195 K. A. Abel, J. C. Boyer and F. C. J. M. van Veggel, *J. Am. Chem. Soc.*, 2009, **131**, 14644–14645.

196 H. Guo, Z. Q. Li, H. S. Qian, Y. Hu and I. N. Muhammad, *Nanotechnology*, 2010, **21**, 125602.

197 D. Dolmans, D. Fukumura and R. K. Jain, *Nat. Rev. Cancer*, 2003, **3**, 380–387.

198 A. P. Castano, P. Mroz and M. R. Hamblin, *Nat. Rev. Cancer*, 2006, **6**, 535–545.

199 B. W. Henderson, S. M. Waldow, T. S. Mang, W. R. Potter, P. B. Malone and T. J. Dougherty, *Cancer Res.*, 1985, **45**, 572–576.

200 D. Dolmans, A. Kadambi, J. S. Hill, C. A. Waters, B. C. Robinson, J. P. Walker, D. Fukumura and R. K. Jain, *Cancer Res.*, 2002, **62**, 2151–2156.

201 V. H. Fingar, P. K. Kik, P. S. Haydon, P. B. Cerrito, M. Tseng, E. Abang and T. J. Wieman, *Br. J. Cancer*, 1999, **79**, 1702–1708.

202 B. P. Shumaker and F. W. Hetzel, *Photochem. Photobiol.*, 1987, **46**, 899–901.

203 G. R. Reddy, M. S. Bhojani, P. McConville, J. Moody, B. A. Moffat, D. E. Hall, G. Kim, Y. E. L. Koo, M. J. Woolliscroft, J. V. Sugai, T. D. Johnson, M. A. Philbert, R. Kopelman, A. Rehemtulla and B. D. Ross, *Clin. Cancer Res.*, 2006, **12**, 6677–6686.

204 P. Zhang, W. Steelant, M. Kumar and M. Scholfield, *J. Am. Chem. Soc.*, 2007, **129**, 4526–4527.

205 D. K. Chatterjee and Y. Zhong, *Nanomedicine*, 2008, **3**, 73–82.

206 B. Ungun, R. K. Prud'homme, S. J. Budijono, J. N. Shan, S. F. Lim, Y. G. Ju and R. Austin, *Opt. Express*, 2009, **17**, 80–86.

207 H. S. Qian, H. C. Guo, P. C. L. Ho, R. Mahendran and Y. Zhang, *Small*, 2009, **5**, 2285–2290.

208 H. C. Guo, H. S. Qian, N. M. Idris and Y. Zhang, *Nanomed.: Nanotechnol., Biol. Med.*, 2010, DOI: 10.1016/j.nano.2009.11.004.

209 Y. Y. Guo, M. Kumar and P. Zhang, *Chem. Mater.*, 2007, **19**, 6071–6072.

210 S. Schietinger, T. Aichele, H. Q. Wang, T. Nann and O. Benson, *Nano Lett.*, 2010, **10**, 134–138.

211 H. T. Wong, H. L. W. Chan and J. H. Hao, *Opt. Express*, 2010, **18**, 6123–6130.